minerals

MDPI

Article

Provenance, Sedimentary Environment, Tectonic Setting, and Uranium Mineralization Implications of the Yaojia Formation, SW Songliao Basin, NE China

Mengya Chen, Fengjun Nie *, Fei Xia, Zhaobin Yan and Dongguang Yang

School of Earth Sciences, East China University of Technology, Nanchang 330013, China; infinitekyu0428@126.com (M.C.)
* Correspondence: niefj@ecit.edu.cn; Tel.: +86-0791-83898009

Abstract: The SW Songliao Basin is an extremely significant part of the giant sandstone uranium metallogenic belt in northern China. The Yaojia Formation is the most significant ore-bearing layer in the region. However, the poorly constrained sedimentology of the Yaojia Formation has substantially hindered the understanding of the basin and the exploration of uranium deposits within it. To determine the sedimentology, provenance, and tectonic setting of the Yaojia Formation in the study area, we conducted petrography, whole-rock geochemical analysis, and electron probe research. Based on the results of the study, it appears that the Yaojia Formation sandstone is predominantly composed of lithic sandstone and feldspar lithic sandstone. Uranium exists in two forms: as independent minerals and as adsorption uranium. Pitchblende is the most common independent uranium mineral, with small amounts of coffinite also occurring. The ratios of Sr/Ba, V/(V+Ni), V/Cr, Ni/Co, and (Cu+Mo)/Zn of the samples indicate that the Yaojia Formation was deposited in a sub- to oxygen-rich freshwater environment with a moderately stratified bottom water body and smooth circulation. The geochemical characteristics of the Yaojia Formation sandstones imply that they are primarily derived from felsic igneous rocks in the upper continental crust in active continental margin and continental island arc environments. According to geochemistry and previous detrital zircon U-Pb chronology studies, the Mesozoic and Late Paleozoic felsic igneous rocks of the southern Great Xing'an Mountains are the principal sources of the Yaojia Formation in the SW Songliao Basin. Besides providing sediments for the study area, the uranium-rich felsic igneous rocks in the source areas also represent a long-term, stable, and ideal source of uranium, suggesting substantial potential for uranium exploration in the study area.

Keywords: geochemistry; provenance; sedimentary environment; Yaojia Formation; Songliao Basin

check for updates

Citation: Chen, M.; Nie, F.; Xia, F.; Yan, Z.; Yang, D. Provenance, Sedimentary Environment, Tectonic Setting, and Uranium Mineralization Implications of the Yaojia Formation, SW Songliao Basin, NE China. *Minerals* **2023**, *13*, 1053. https://doi.org/10.3390/min13081053

Academic Editors: Davide Lenaz and Sergey V. Krivovichev

Received: 17 May 2023
Revised: 20 July 2023
Accepted: 7 August 2023
Published: 9 August 2023

Copyright: © 2023 by the authors. Licensee MDPI, Basel, Switzerland. This article is an open access article distributed under the terms and conditions of the Creative Commons Attribution (CC BY) license (https://creativecommons.org/licenses/by/4.0/).

1. Introduction

The provenance analysis is essential for determining the nature of the sedimentary basin [1–5]. The geochemical composition analysis of sediments is one of the most sensitive and effective tools for determining the provenance, weathering conditions, tectonic background, and sedimentary environment of the sediments of interest [6,7]. Elemental enrichment, storage, and sedimentary environments are distinct among strata with differing lithologies [8,9]. The homogeneous texture and high trace element concentration of sandstones and mudstones make them preferred for geochemical research on sedimentary rocks [10]. With the help of geochemistry analysis, many remarkable achievements have been made in recent years in identifying the provenance and sedimentary environment of sandstones, thus providing a new perspective for understanding the nature and evolution of basins and source areas [11–13].

The Songliao Basin is a significant part of the giant sandstone uranium metallogenic belt in northern China [14]. Several industrial-grade uranium deposits (such as the Dalin uranium deposit, the Baolongshan uranium deposit, and the Hailijin uranium deposit)

have been discovered in the study area. The uranium deposits in the region are generally considered to be interstratified oxidized-zone sandstone-type deposits [15,16]. In the region, the Yaojia Formation is the most significant uranium-bearing rock series. The numerous studies that have been conducted on sedimentary facies, mineral paragenesis, tectonic setting, metallogenic mechanism, and metallogenic age have significantly increased the potential for uranium exploration in the research area [17–24]. Previous research has concluded that uranium deposits are the products of long-term weathering and erosion of uranium-rich source rocks in the provenance. The process has transported uranium from the source rocks to the sedimentary basin in oxygenated uranium-bearing fluids, which then precipitated into the ore-bearing layers [18,25–29]. Consequently, provenance plays a key role in the formation of sandstone-type uranium deposits, as it provides the necessary uranium-rich clastic materials and oxygenated uranium-bearing fluids. By elucidating sediment sources and sedimentary transport pathways, accurate predictions and evaluations can be made for the exploration of sandstone-type uranium deposits [27]. Despite numerous studies in this region, there has always been controversy regarding the provenance of the Yaojia Formation. Recently, scholars have generally believed that the Yaojia Formation sediments originated from felsic igneous rocks from the Yanshan orogenic belt in the south of the basin [18,27,29]. Alternatively, some scholars believe that the Great Xing'an Mountains in the west of the basin and the Zhangguangcai Mountains in the southeast contributed clastic materials to the Yaojia Formation [28,30,31]. There have been a few elementary investigations into the lithological properties of the Yaojia Formation sandstones [15,18,27–29]. However, there is still a need for refinement of information regarding the source of sediments, particularly in identifying the types of source rocks. Moreover, few studies have been conducted on the provenance of the Yaojia Formation from a geochemical perspective.

Therefore, the purpose of this paper is to identify the provenance, tectonic context, sedimentary environment, and uranium metallogenesis of the Yaojia Formation sandstones in the SW Songliao Basin through a combination of petrology, geochemistry, and electron-probe analysis. The study is expected to assist in understanding the mineralization mechanism of the uranium deposits and the next phase of exploration in the basin.

2. Geological Setting

The Songliao Basin is a strip-shaped Mesozoic rifted sedimentary basin that developed on the folded basement of the Paleozoic geosyncline [15,32,33] (Figure 1a). The Songliao Basin is surrounded tectonically by a series of mountains, with the Zhangguangcai Mountains (ZGCM) in the southeast and the Lesser Xing'an Mountains (LXAM) in the northeast, both of which developed Late Triassic to Middle Jurassic igneous rocks [34–36]; the Great Xing'an Mountains (GXAM) in the west, which mainly developed Late Paleozoic and Mesozoic granites and volcanic rocks [37–39]; and the Kangfa Hill areas in the south, which are part of the Yanshan orogenic belt in the northern margin of the North China Craton [40]. As the main sources of the Songliao Basin, these mountains have played a significant role in its evolution and development [27–31]. The study area is situated southwest of the Songliao Basin and is one of the seven basin's structural units (Figure 1b).

The basin's basement consists mostly of Precambrian to Palaeozoic metamorphic rocks, Palaeozoic to Mesozoic granites, Palaeozoic sedimentary strata, and Late Jurassic intermediate-felsic volcanic rocks [15,41–44] (Figure 1c). The Cretaceous deposits that cover the entire study area constitute the principal sedimentary caprocks. The Songliao Basin was formed and filled through four tectonic phases [20] (Figure 2): mantle upwelling, rifting, post-rift thermal subsidence, and structural inversion. In these four phases, three major tectonostratigraphic sequences were generated [14,45–47]: (i) The pre-rift and syn-rift tectonostratigraphic sequences (150–125 Ma), composed of the Huoshiling (J_3h), Shahezi (K_1sh), and Yingcheng (K_1yc) Formations, were formed in separate rift grabens [20]. (ii) The post-rift tectonostratigraphic sequences (125–79.1 Ma) consist of the Dengloukou (K_1d), Quantou ($K_{1\text{-}2}q$), Qingshankou (K_2qn), Yaojia (K_2y), and Nenjiang (K_2n) Forma-

tions [20]; (iii) the tectonic inversion sequences (79.1–23 Ma) consist of the Sifangtai (K_2s), Mingshui (K_2m), and Yi'an Formations ($E_{2\text{-}3}y$) [20,22].

The Yaojia Formation is a set of 100–200 m thick inland clastic sedimentary formations widely distributed in the region. The burial depth of the Yaojia Formation is generally 300–600 m and can be greater than 800 m locally. In general, it is comprised of sandy conglomerates, gray, gray-white medium- to coarse-grained sandstones, purplish-red siltstones, and reddish-purple mudstones [48]. According to exploration in the study area, uranium mineralization is mainly found in coarse-grained sandbodies of the Yaojia Formation [21,26].

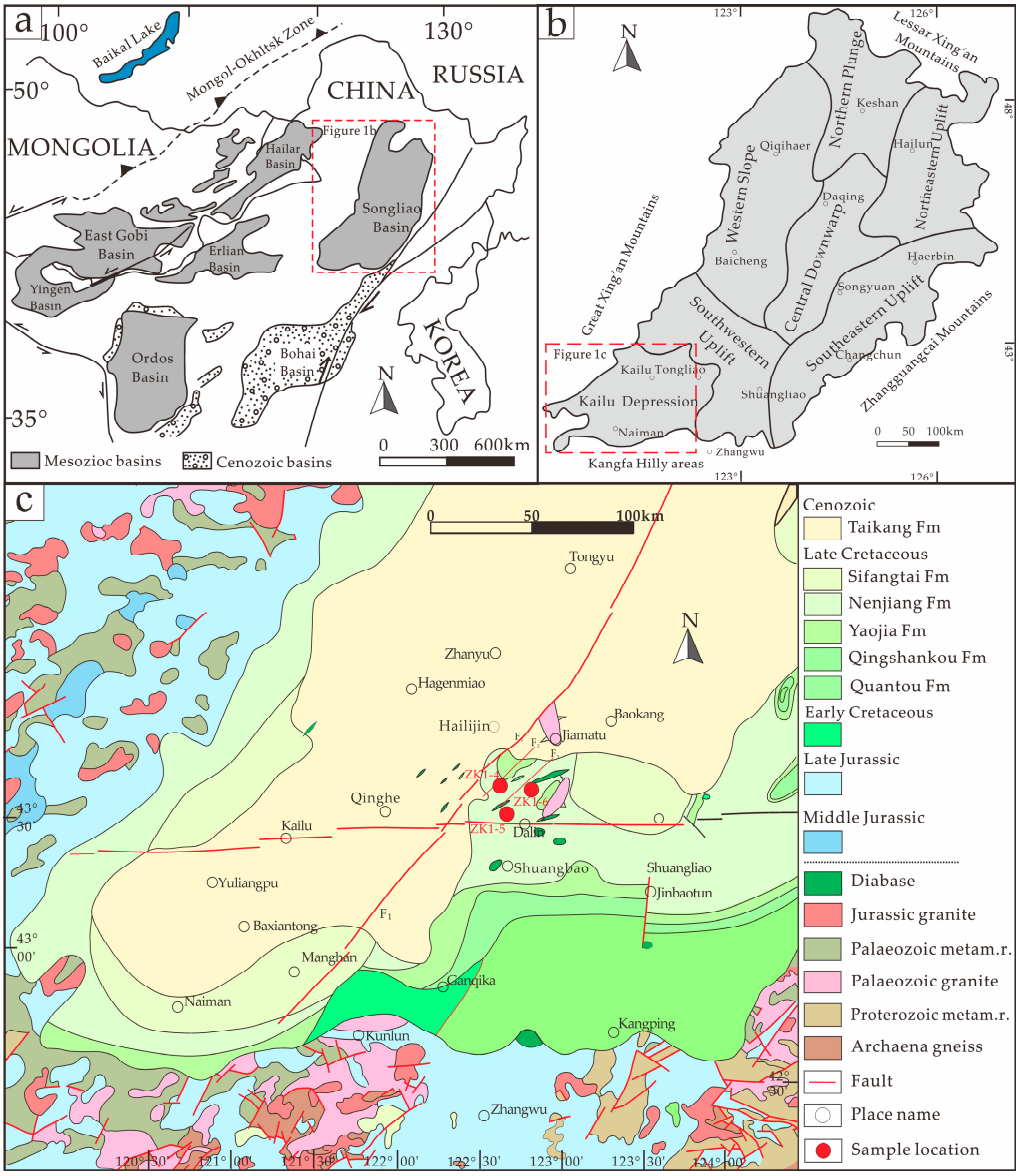


Figure 1. Geological maps of the Songliao Basin and the study area. (**a**) Structural map of northeast China (modified after Bonnetti et al. [20]); (**b**) Structural map of the Songliao Basin (modified after Scott et al. [49]; Zhao et al. [50]); (**c**) Geological map of the SW Songliao Basin.

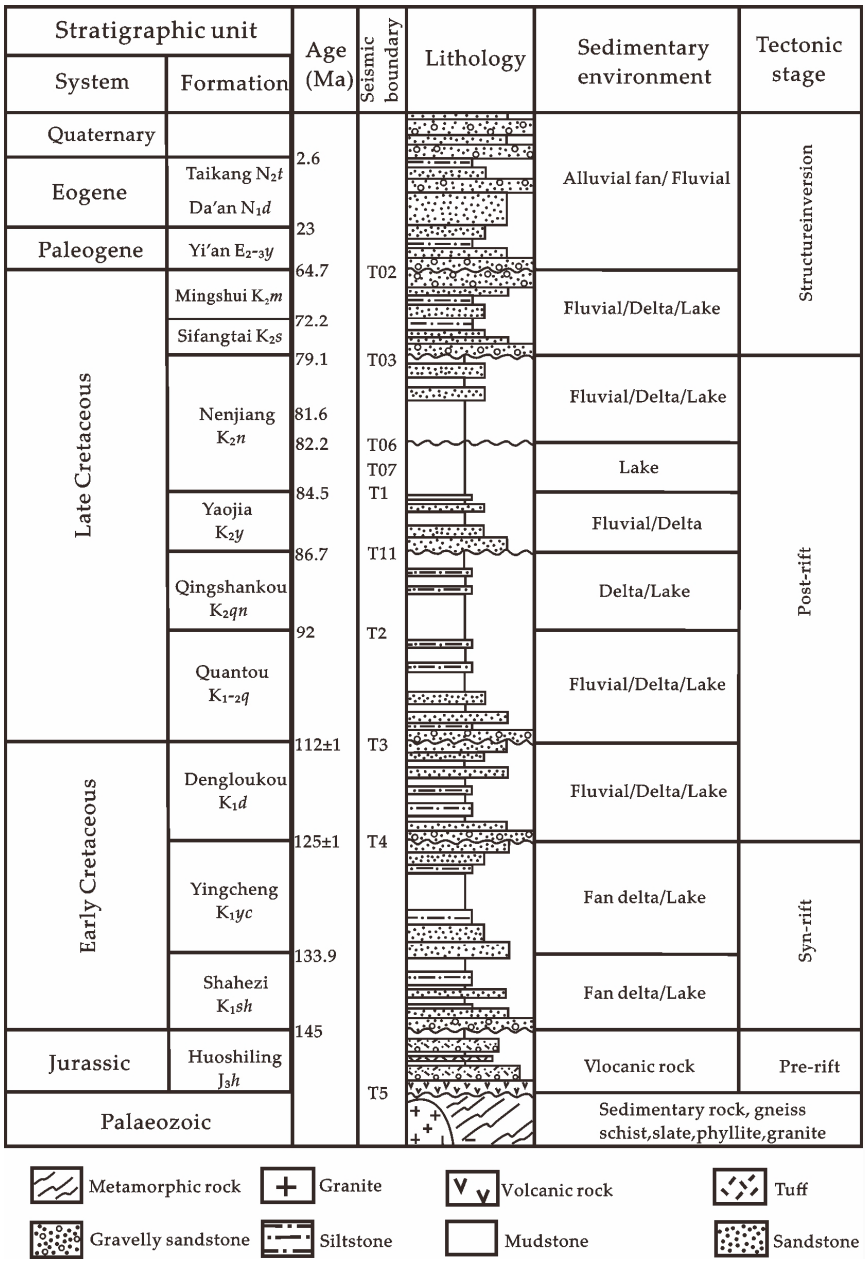


Figure 2. Palaeozoic to Cenozoic tectono-stratigraphic evolution of the Songliao Basin (modified after Bonnetti et al. [20]).

3. Samples and Materials

Twenty fresh sandstone samples of the Yaojia Formation were collected from three representative drill holes (ZK1-4, ZK1-6, and ZK1-5) in the study area (Figure 1). Table 1 and Figure 3 provide details about the sampling sites. These samples were primarily composed of gray-white or light-red, medium-grained sandstones. The samples were examined using a combination of thin-section identification, whole-rock geochemistry, and electron probe analysis.

Table 1. Details of sandstone samples from the Yaojia Formation in the SW Songliao Basin.

Sample	Drill Hole	Depth	Lithology
KL051	ZK1-4	599.6 m	Gray-white medium-grained sandstone
KL052	ZK1-4	599.4 m	Light red medium-grained sandstone
KL053	ZK1-4	599.3 m	Gray-white medium-grained sandstone
KL054	ZK1-4	599.1 m	Gray-white medium-grained sandstone
KL056	ZK1-6	593.7 m	Gray-white medium-grained sandstone
KL057	ZK1-6	593.5 m	Light red medium-grained sandstone
KL058	ZK1-6	593.4 m	Gray-white medium-grained sandstone
KL059	ZK1-6	592.5 m	Gray-white medium-grained sandstone
KL060	ZK1-6	590.3 m	Gray-white medium-grained sandstone
KL061	ZK1-6	576.6 m	Gray-white medium-grained sandstone
KL062	ZK1-6	586.9 m	Light red medium-grained sandstone
KL063	ZK1-6	585.6 m	Light red medium-grained sandstone
KL066	ZK1-5	562.3 m	Light red medium-grained sandstone
KL067	ZK1-5	561.9 m	Gray-white medium-grained sandstone
KL068	ZK1-5	558.4 m	Gray-white medium-grained sandstone
KL069	ZK1-5	546.1 m	Gray-white medium-grained sandstone
KL070	ZK1-5	539.7 m	Gray-white coarse-grained sandstone
KL071	ZK1-5	526.0 m	Gray-white medium-grained sandstone
KL072	ZK1-5	514.9 m	Light red fine-grained sandstone
KL073	ZK1-5	473.3 m	Light red medium-grained sandstone

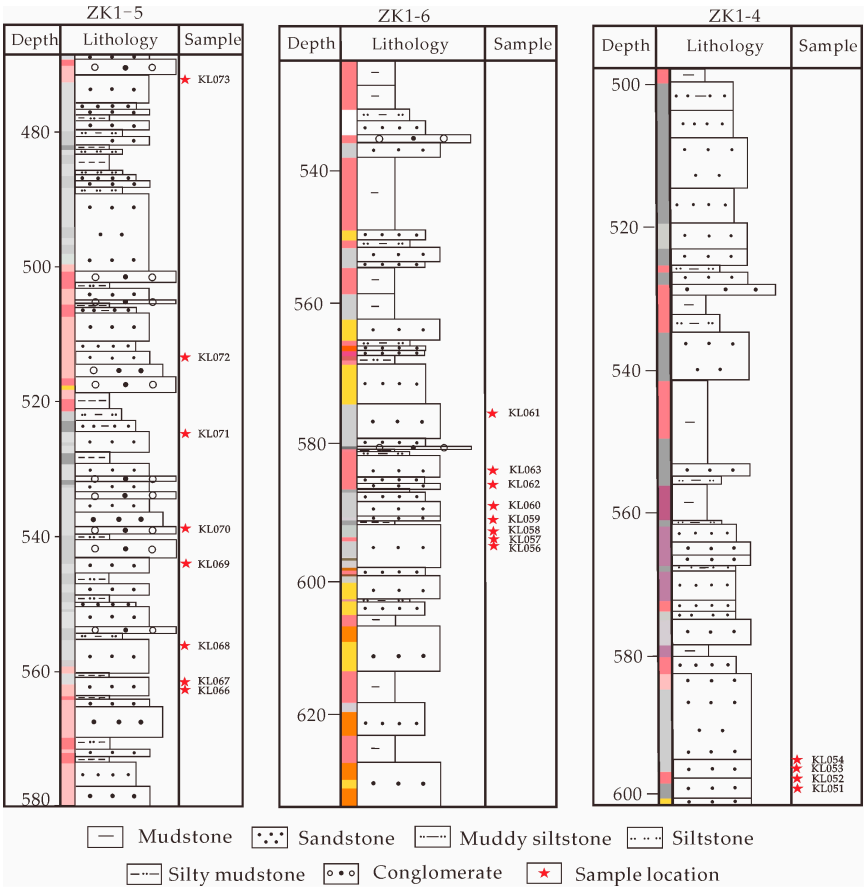


Figure 3. The distribution and location of samples in the drill holes.

The thin-section petrographic identification was performed using a Nikon 100 N electron microscope in the electron microscopy laboratory of the East China University of Technology. At least 300 grains have been counted in each thin section. The Gazzi-Dickinson method was used to analyze the sandstone's characteristics [51].

The whole-rock geochemistry analysis was conducted at the Beijing Test and Analysis Center of the Nuclear Industry. Fresh samples were pulverized to 200 mesh for later work after the removal of altered surfaces. The major elements were assayed with an X-ray fluorescence spectrometer (XRF). Axios-Max XRF was used for testing the prepared samples, and the method used was ME-XRF26D. Blank, duplicate, and standard samples (GBW07105, NCSDC47009, SARM-4, and SARM-5) were used for monitoring during the testing process. In general, the analytical accuracy was greater than 5%, and the detection limit was less than 0.01%. Loss of ignition was assessed by heating the sample powder to 1000 °C for one hour [52].

At the Beijing Test and Analysis Center of the Nuclear Industry, trace elements were assayed with a NexION 300D ICP-MS. In a Teflon container, approximately 50 mg of whole rock powder was dissolved in HNO_3-HF distillate. The solution was maintained at 185 °C for three days in an oven. Once the HF had been evaporated from the solution, deionized water was used to dilute the final solution to 100.0 g after adding the Rh internal standard solution, so that the concentration of Rh in the final solution became 10 ng/mL. The elemental composition of the solution was determined by ICP-MS. Overall, the precision was greater than 5%.

Representative ore-bearing samples were selected and subjected to electron microprobe experiments for uranium mineral composition identification. The electron probe experiment was conducted at the State Key Laboratory of Nuclear Resources and Environment, East China University of Technology, Jiangxi Province, China. The instrument used in the experiment is the JXA-8100M electron probe and its accompanying IncaEnergy spectrometer. The test conditions are: an acceleration voltage of 15.0 kV, a probe current of 20.0 nA, and a beam spot diameter <2 μm. The testing procedure was conducted in accordance with the national standard (GB/T 15617-2002) [53].

4. Results

4.1. Petrography

Petrological characteristics indicate that the detrital particles are poorly sorted, with sub-angular to angular roundness (Figure 4), which is indicative of proximal deposition. Table 2 provides statistics on the mineral composition of sandstone clasts. According to a petrological investigation, it was determined that the Yaojia Formation sandstone is predominantly composed of lithic sandstone and feldspar lithic sandstone. There are approximately 80%–90% grains in the sandstone, predominantly quartz, feldspar, and lithic fragments. It is noteworthy that the content of lithic fragments ranges from 24% to 68%; the content of quartz ranges from 24% to 61%; and the content of feldspar ranges from 8% to 16%. Quartz is dominated by monocrystalline quartz, most of which has eroded edges with no wavy extinction and other characteristics, indicating a volcanic origin (Figure 4a,b). Feldspar consists mostly of potassium feldspar and plagioclase, the majority of which has been sericitized (Figure 4c). There is a wide variety of lithic fragments, including felsic volcanic lithic fragments, granite fragments, polycrystalline quartz fragments, and a small amount of metamorphic lithic fragments (Figure 4d–f). The cements are well-developed in the sandstones, with a content of 8% to 15%. Carbonate, clay minerals, and ferruginous cement comprise the majority of cements. The carbonates are primarily composed of calcite and dolomite. Calcite metasomatizes quartz and feldspar frequently (Figure 5a). The dominant clay mineral is kaolinite, which develops between detrital particles in the form of fish scales or book leaves (Figure 5b). There is also a small amount of illite and chlorite present. Ferruginous cement is primarily composed of hematite and limonite. Pyrite and organic matter are also common in the studied samples. Pyrite is developed in framboidal, colloidal, or euhedral-sub-euhedral forms (Figure 5c,d). The organic matter is primarily composed of carbonaceous fragments and bitumen (Figure 5e,f). Pyrite is visible occupying the cell cavities of carbonaceous fragments. In the Qt-F-L and Qm-F-Lt discrimination diagrams, the Yaojia Formation samples fall into the recycled orogenic and transitional arc regions (Figure 6).

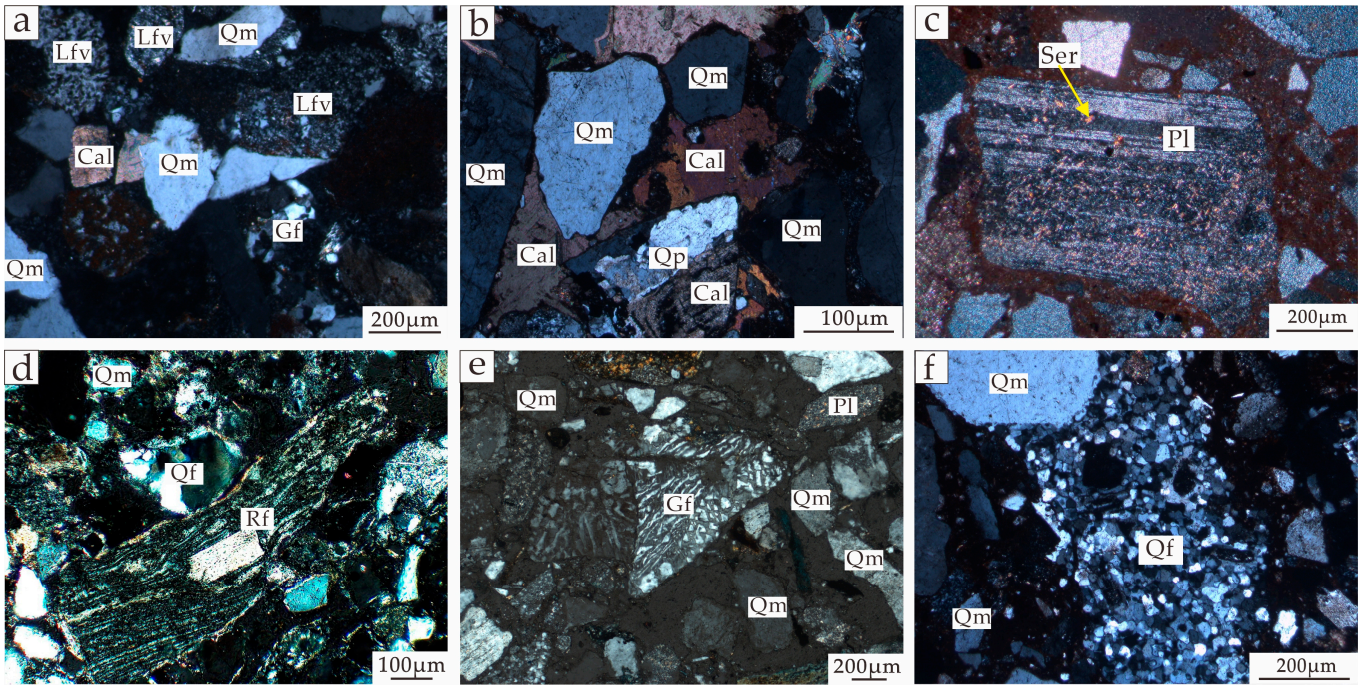


Figure 4. Photomicrographs of the Yaojia Formation sandstones. (**a**) Sandstone with felsic volcanic lithic fragments, monocrystalline quartz, granite fragments, and calcite (+). (**b**) Monocrystalline quartz and polycrystalline quartz are metasomatized by calcite (+). (**c**) Sericitization of plagioclase (+). (**d**) Quartz fragment and rhyolite fragment (+). (**e**) Granite fragment (+). (**f**) Quartz fragment (Qf). (+) = cross-polarized light. Abbreviations: Lfv, felsic volcanic lithic fragment; Qm, monocrystalline quartz; Cal, calcite; Gf, granite fragments; Qp, polycrystalline quartz; Pl, plagioclase; Ser, Sericitization; Qf, quartz fragment; Rf, rhyolite fragment.

Table 2. Statistics of detrital grains from sandstone samples in the SW Songliao Basin.

Sample	Lithology	Qm (%)	Qp (%)	Qt (%)	F (%)	L (%)	Lt (%)
KL051	Gray-white medium-grained sandstone	44	8	52	9	39	47
KL052	Light red medium-grained sandstone	34	6	40	12	48	54
KL053	Gray-white medium-grained sandstone	28	9	37	10	53	62
KL054	Gray-white medium-grained sandstone	19	6	25	16	59	65
KL056	Gray-white medium-grained sandstone	20	4	24	8	68	72
KL057	Light red medium-grained sandstone	35	7	42	9	49	56
KL058	Gray-white medium-grained sandstone	28	6	34	9	57	63
KL059	Gray-white medium-grained sandstone	25	8	33	8	59	67
KL060	Gray-white medium-grained sandstone	49	12	61	15	24	36
KL061	Gray-white medium-grained sandstone	41	8	49	10	41	49
KL062	Light red medium-grained sandstone	25	7	32	11	57	64
KL063	Light red medium-grained sandstone	33	11	44	9	47	58
KL066	Light red medium-grained sandstone	28	5	33	13	54	59
KL067	Gray-white medium-grained sandstone	30	5	35	12	53	58
KL068	Gray-white medium-grained sandstone	26	4	30	13	57	61
KL069	Gray-white medium-grained sandstone	41	6	47	14	39	45
KL070	Gray-white coarse-grained sandstone	33	3	36	8	56	59
KL071	Gray--white medium-grained sandstone	35	5	40	10	50	55
KL072	Light red fine-grained sandstone	30	4	34	9	57	61
KL073	Light red medium grained-sandstone	51	5	56	8	36	41

Note: Qm = Monocrystalline quartz; Qp = Polycrystalline quartz; Qt = Total quartz; F = Feldspar; L = Lithic clasts; Lt = L + Qp.

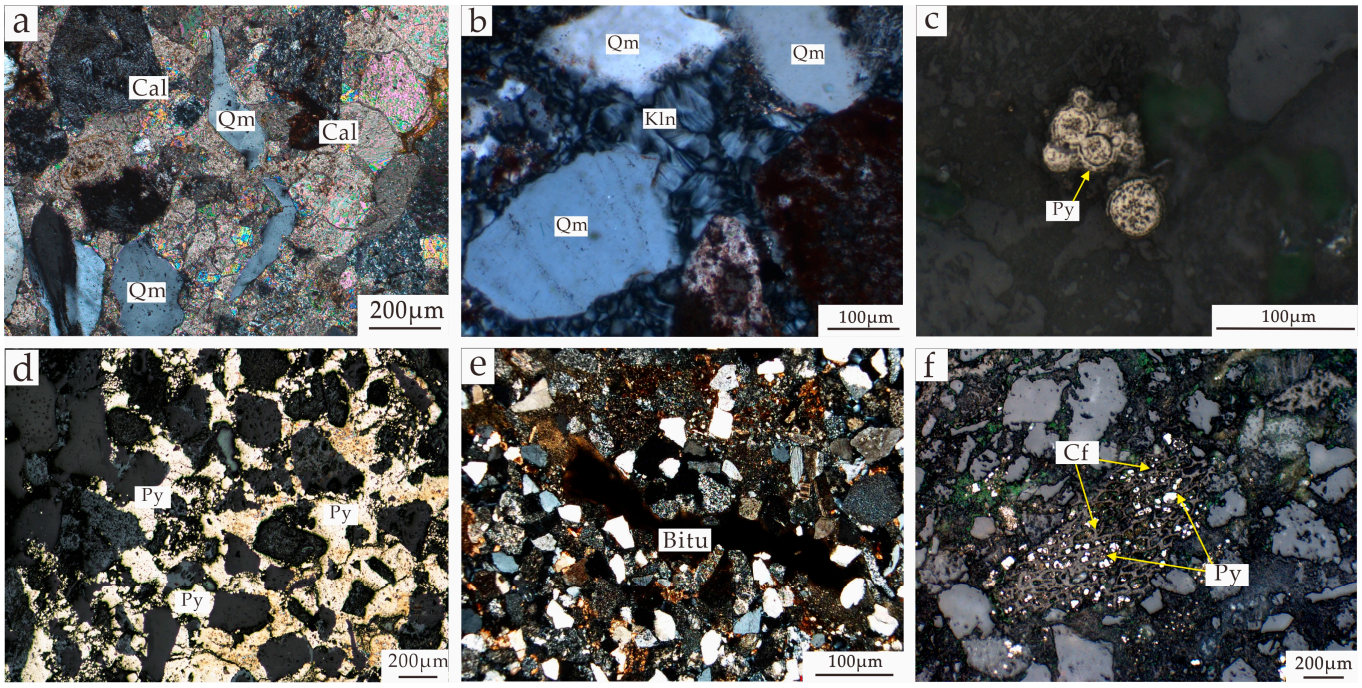


Figure 5. Photomicrographs of the Yaojia Formation sandstones. (**a**) Calcite metasomatizes quartz (+). (**b**) Kaolinite developed between the detrital particles in the form of a book leaf (+). (**c**) Framboidal pyrite (RL). (**d**) Colloidal pyrite (RL). (**e**) Bitumen (+). (**f**) Pyrite occupies the cell cavities of carbonaceous fragments (RL). (+) = cross-polarized light; (RL) = reflected light. Abbreviations: Qm, monocrystalline quartz; Cal, calcite; Kln, kaolinite; Py, pyrite; Bitu, bitumen; Cf, carbonaceous fragments.

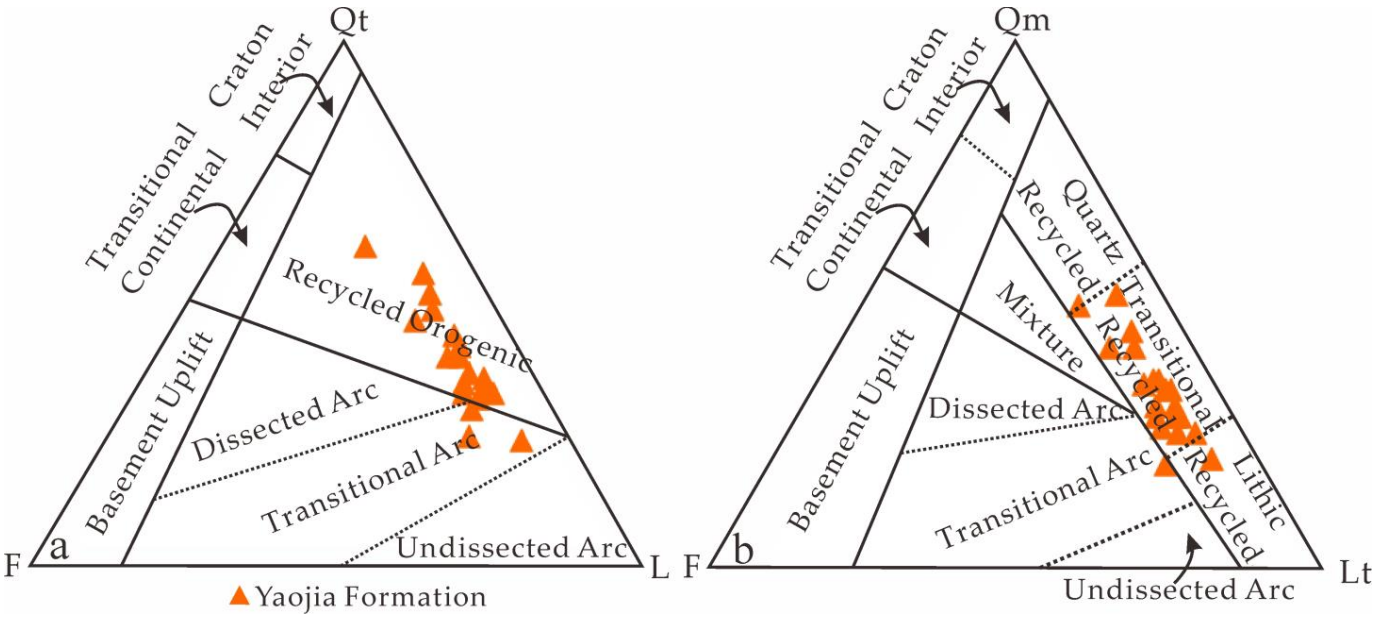


Figure 6. (**a**) Qt-F-L and (**b**) Qm-F-Lt discrimination diagrams of the Yaojia Formation in the SW Songliao Basin (after Dickinson and Suczek [51]).

4.2. Geochemistry

4.2.1. Major Elements

The geochemical characteristics of major elements in the Yaojia Formation samples are listed in Table 3. The most abundant element in the samples was SiO_2, indicating

that the sandstones are rich in quartz or silica-containing minerals. The SiO_2 content in these samples ranges from 50.44% to 81.49% (avg. 72.95%). The Al_2O_3 content of sandstone is an effective indicator of clay alteration. The Al_2O_3 content of the samples ranges from 7.14% to 13.09% (avg. 10.04%), indicating that they had been subjected to relatively strong alteration. The $Fe_2O_3{}^T$ content ranges from 0.74% to 4.86% (avg. 2.24%); the MgO content ranges from 0.24% to 5.45% (avg. 1.36%); the CaO content ranges from 0.14% to 11.65% (avg. 2.87%); the Na_2O content ranges from 0.13% to 1% (avg. 0.48%); the K_2O content ranges from 2.39% to 3.39% (avg. 3.02%); the MnO content ranges from 0 to 0.30% (avg. 0.07%); the TiO_2 content ranges from 0.18% to 0.58% (avg. 0.31%); the P_2O_5 content ranges from 0.06% to 0.49% (avg. 0.11%); the average SiO_2+Al_2O_3 content is 82.99%; the average SiO_2/Al_2O_3 ratio is 7.30; the average K_2O+Na_2O content is 3.49%; and the average K_2O/Na_2O ratio is 8.93. The loss on ignition (LOI) content varies widely, ranging from 2.60% to 17.03% (avg. 6.45%). The cause of this phenomenon may be due to a high carbonate content or to later weathering. The indices of chemical weathering, CIA (Chemical Index of Alternation) [54], CIW (Chemical Index of Weathering) [55], and ICV (Index of Compositional Variability) [56], range from 58.41 to 74.80 (avg. 67.80), from 74.52 to 95.74 (avg. 87.08), and from 0.63 to 3.15 (avg. 1.09), respectively.

4.2.2. Trace Elements

Table 4 lists the results of tests conducted on trace elements in the samples. The large ion lithophile elements such as Cs, Rb, Sr, and Ba have average contents of 4.93 ppm, 101.48 ppm, 223.94 ppm, and 693.40 ppm, respectively. High field strength elements such as Sc, Y, Nb, Ta, Zr, Hf, and Th have average contents of 4.29 ppm, 23.36 ppm, 10.95 ppm, 0.84 ppm, 100.39 ppm, 3.13 ppm, and 9.19 ppm, respectively. The normalized trace elements of the upper continental crust (UCC) with reference to Taylor and McLennan (1985) [6] were applied, and the curve patterns were almost identical across all samples, with abundances approximately the same as those of the upper crustal elements (Figure 7). Moreover, these samples are extremely abundant in U, indicating a significant potential for mineralization. According to the average ratios of La/Sc, Th/Sc, Cr/Th, and Co/Th, the provenance is mainly situated in the upper crustal felsic source area [6,57] (Table 5).

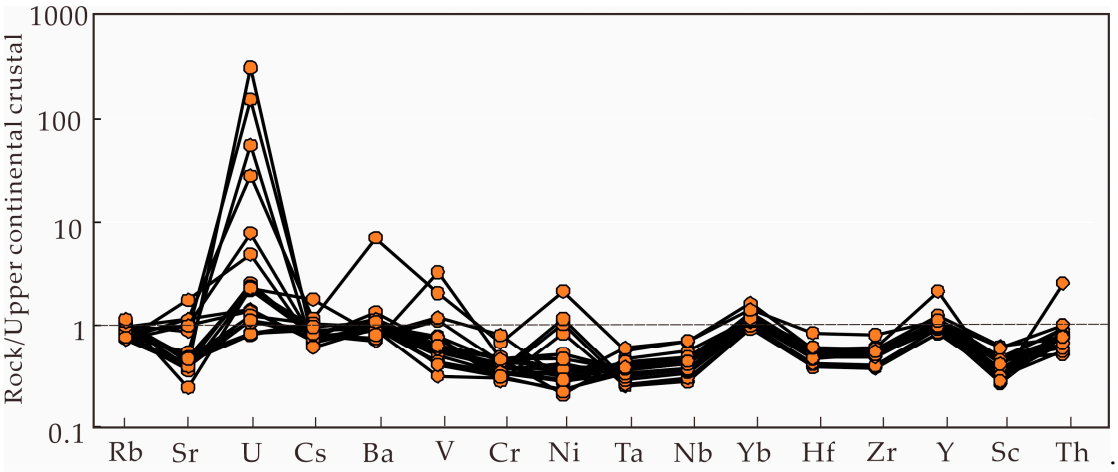


Figure 7. Upper continental crustal normalized trace element spider diagram of the Yaojia Formation sandstones.

Table 3. Data table of major element analysis of the Yaojia Formation sandstones in the SW Songliao Basin (wt%).

Sample	SiO_2	Al_2O_3	$Fe_2O_3^T$	MgO	CaO	Na_2O	K_2O	MnO	TiO_2	P_2O_5	LOI	Total	SiO_2+ Al_2O_3	SiO_2/ Al_2O_3	K_2O+ Na_2O	K_2O/ Na_2O	CIA	CIW	ICV
KL051	77.02	10.42	1.73	0.67	1.45	0.49	3.31	0.04	0.30	0.08	4.48	99.99	87.44	7.39	3.80	6.76	66.68	86.53	0.81
KL052	76.83	10.46	1.65	0.69	1.48	0.53	3.37	0.04	0.25	0.07	4.61	99.98	87.29	7.35	3.90	6.36	65.97	85.69	0.82
KL053	79.09	9.77	1.29	0.55	1.21	0.44	3.16	0.03	0.26	0.08	4.05	99.93	88.86	8.10	3.60	7.18	66.72	87.07	0.77
KL054	80.16	9.98	0.87	0.43	0.88	0.43	3.23	0.03	0.21	0.07	3.69	99.98	90.14	8.03	3.66	7.51	67.00	87.56	0.69
KL056	50.44	7.14	4.67	5.45	11.63	0.74	2.44	0.30	0.18	0.07	16.90	99.96	57.58	7.06	3.18	3.30	58.41	74.52	3.15
KL057	51.24	7.65	3.49	5.30	11.61	0.71	2.46	0.21	0.21	0.08	17.03	99.99	58.89	6.70	3.17	3.46	60.46	76.58	2.77
KL058	51.68	7.68	3.30	5.20	11.65	0.70	2.39	0.22	0.23	0.07	16.85	99.97	59.36	6.73	3.09	3.41	61.09	76.93	2.70
KL059	74.72	9.78	1.93	1.22	2.46	0.81	3.10	0.09	0.27	0.10	5.49	99.97	84.50	7.64	3.91	3.83	61.89	78.58	1.11
KL060	81.49	10.12	0.78	0.24	0.37	0.54	3.24	0.02	0.38	0.12	2.60	99.90	91.61	8.05	3.78	6.00	67.98	88.95	0.63
KL061	70.37	12.05	4.86	0.24	0.14	0.39	3.19	0.00	0.58	0.49	6.20	98.51	82.42	5.84	3.58	8.18	71.85	90.49	0.76
KL062	78.14	10.71	1.55	0.52	1.05	0.57	3.28	0.02	0.29	0.07	3.76	99.96	88.85	7.30	3.85	5.75	66.40	85.14	0.76
KL063	79.60	9.79	1.40	0.52	1.09	0.53	3.18	0.03	0.28	0.06	3.47	99.95	89.39	8.13	3.71	6.00	65.38	84.90	0.80
KL066	73.54	9.73	3.35	1.13	2.47	0.17	2.65	0.10	0.34	0.10	6.40	99.98	83.27	7.56	2.82	15.59	74.03	94.72	0.92
KL067	78.67	10.07	2.86	0.36	0.44	0.16	2.77	0.04	0.35	0.11	4.14	99.97	88.74	7.81	2.93	17.31	74.01	94.94	0.67
KL068	74.57	9.97	2.29	1.11	2.73	0.14	2.67	0.09	0.33	0.09	5.95	99.94	84.54	7.48	2.81	19.07	74.80	95.52	0.82
KL069	75.47	11.49	1.73	0.80	1.46	0.19	3.09	0.03	0.33	0.11	5.28	99.98	86.96	6.57	3.28	16.26	74.32	94.84	0.66
KL070	79.88	9.46	1.51	0.62	1.15	0.13	2.81	0.04	0.27	0.09	4.03	99.99	89.34	8.44	2.94	21.62	73.20	95.74	0.67
KL071	71.97	11.20	2.20	1.23	2.58	0.29	3.35	0.03	0.32	0.09	6.68	99.94	83.17	6.43	3.64	11.55	70.91	92.05	0.85
KL072	79.44	10.21	0.74	0.51	1.17	0.55	3.39	0.04	0.24	0.09	3.59	99.97	89.65	7.78	3.94	6.16	65.08	84.97	0.74
KL073	74.70	13.09	2.59	0.43	0.37	1.00	3.27	0.02	0.56	0.08	3.81	99.92	87.79	5.71	4.27	3.27	69.74	85.96	0.70

Table 4. Data table of trace element analysis of the Yaojia Formation sandstones in the SW Songliao Basin (ppm).

Sample	Li	Be	Sc	V	Cr	Co	Ni	Cu	Zn	Ga	Rb	Sr	Y	Mo	Cd
KL051	45.90	1.90	3.70	32.20	13.60	3.92	7.17	3.85	36.80	13.20	117.00	151.00	23.70	0.89	0.13
KL052	46.20	1.88	3.60	30.00	11.80	4.00	6.85	3.44	34.00	12.70	117.00	150.00	23.30	0.74	0.12
KL053	46.70	1.71	3.36	24.50	12.10	3.38	5.75	4.23	31.60	12.70	113.00	166.00	22.40	0.62	0.10
KL054	44.90	1.52	2.92	18.90	10.50	2.79	4.61	4.90	24.00	12.20	109.00	157.00	20.40	0.49	0.10
KL056	19.40	3.01	5.02	46.20	9.86	10.60	16.50	3.64	68.70	9.50	81.20	611.00	18.10	0.56	0.36
KL057	18.80	2.03	3.45	36.60	11.50	14.40	20.40	3.62	85.20	9.35	82.30	393.00	18.40	0.49	0.37
KL058	18.40	1.90	5.05	38.10	12.40	16.00	22.90	3.71	92.50	9.47	81.10	340.00	20.30	0.50	0.42
KL059	21.30	1.34	5.01	43.30	12.70	5.63	8.23	5.44	49.10	11.10	94.90	173.00	21.80	0.56	0.14
KL060	25.30	1.86	3.01	35.40	16.20	1.67	4.10	6.55	47.10	12.40	111.00	302.00	21.40	0.63	0.11

Table 4. *Cont.*

Sample	Li	Be	Sc	V	Cr	Co	Ni	Cu	Zn	Ga	Rb	Sr	Y	Mo	Cd
KL061	31.50	3.17	3.23	123.00	23.40	37.20	42.80	12.40	41.00	19.20	108.00	392.00	46.90	21.20	0.70
KL062	33.90	1.60	5.08	35.00	14.60	3.24	5.37	4.35	34.80	12.90	114.00	161.00	24.30	0.92	0.17
KL063	35.20	1.40	5.34	38.30	13.50	5.52	6.12	5.05	35.70	12.20	112.00	133.00	25.00	0.70	0.23
KL066	28.60	1.43	6.73	196.00	16.30	7.40	10.10	5.58	64.10	11.20	85.10	147.00	27.10	0.82	0.37
KL067	28.40	1.54	3.63	65.70	14.90	7.81	7.74	9.92	41.20	11.20	86.60	124.00	23.30	0.54	0.10
KL068	17.80	1.90	4.10	45.40	15.10	5.19	10.40	7.38	51.30	11.50	80.60	136.00	22.00	54.90	0.35
KL069	24.10	1.31	5.00	37.10	16.90	4.55	7.35	5.37	37.60	12.80	95.90	341.00	20.10	1.23	0.11
KL070	14.60	1.41	3.44	26.20	11.90	3.01	5.52	4.09	31.50	10.50	84.80	187.00	20.60	0.64	0.12
KL071	24.70	1.37	4.54	37.50	16.00	4.79	9.20	4.09	46.50	13.40	110.00	168.00	22.50	0.62	0.10
KL072	29.20	1.40	3.09	24.20	10.80	2.25	4.41	5.30	25.00	12.80	119.00	162.00	21.30	0.55	0.16
KL073	35.80	2.45	6.46	70.00	27.50	2.69	5.77	17.40	38.30	18.10	127.00	84.80	24.20	0.98	0.06

Sample	In	Sb	Cs	Ba	W	Tl	Pb	Bi	Th	U	Nb	Ta	Zr	Hf
KL051	0.03	1.40	5.69	524.00	1.68	0.73	16.60	0.14	8.92	2.21	11.90	0.92	98.70	3.26
KL052	0.03	1.28	5.71	513.00	1.48	0.74	15.70	0.09	8.72	2.30	10.50	0.82	97.40	3.22
KL053	0.03	1.21	4.94	508.00	1.43	0.69	17.10	0.08	9.13	2.29	11.10	0.86	98.80	3.24
KL054	0.03	1.12	4.29	487.00	1.26	0.66	17.40	0.07	8.38	3.10	9.30	0.74	92.80	3.00
KL056	0.02	1.77	3.68	532.00	1.24	0.48	15.60	0.07	5.51	13.60	6.87	0.55	71.60	2.24
KL057	0.02	1.27	3.90	490.00	1.06	0.48	16.70	0.05	5.88	3.92	7.51	0.58	73.70	2.38
KL058	0.02	1.06	3.96	540.00	1.22	0.51	17.10	0.06	6.30	3.77	8.50	0.64	75.20	2.42
KL059	0.03	1.26	4.80	568.00	1.32	0.58	14.80	0.10	7.84	2.94	8.97	0.68	103.00	3.20
KL060	0.04	1.35	4.41	627.00	1.95	0.72	24.90	0.17	10.70	440.00	13.70	1.03	92.40	2.79
KL061	0.03	3.51	6.45	3890.00	2.58	4.17	100.00	0.24	27.50	78.90	17.10	1.22	114.00	3.29
KL062	0.03	1.36	5.77	512.00	1.69	0.72	20.30	0.11	9.68	3.49	11.70	0.92	102.00	3.46
KL063	0.03	1.78	4.96	501.00	1.60	0.71	19.20	0.11	9.63	3.08	12.00	0.96	99.90	3.27
KL066	0.04	1.32	4.54	384.00	1.90	0.52	14.20	0.11	7.90	7.16	10.90	0.79	110.00	3.25
KL067	0.03	1.11	4.40	409.00	1.42	0.52	16.80	0.11	8.13	6.16	10.80	0.81	109.00	3.31
KL068	0.03	2.21	3.79	506.00	1.66	0.63	16.10	0.16	8.46	898.00	10.20	0.79	109.00	2.66
KL069	0.03	0.96	4.09	729.00	1.40	0.62	15.30	0.08	6.95	22.00	10.30	0.79	97.40	3.04
KL070	0.02	1.12	3.36	496.00	1.13	0.53	13.10	0.08	7.06	157.00	9.14	0.72	97.90	2.72
KL071	0.03	1.02	4.57	626.00	1.46	0.63	13.60	0.12	8.19	6.70	10.20	0.80	110.00	3.46
KL072	0.03	1.18	5.32	588.00	1.36	0.74	16.10	0.15	8.15	6.36	10.90	0.83	104.00	3.50
KL073	0.07	1.76	10.00	438.00	3.11	0.79	15.80	0.32	10.70	6.40	17.40	1.29	151.00	4.81

Table 5. Trace element ratios of the Yaojia Formation sandstones in the SW Songliao Basin.

Ratio	Yaojia Formation	Mafic Provenance	Felsic Provenance	Upper Crust	Lower Crust
La/Sc	7.34	0.40~1.10	2.50~16.00	2.70	0.30
Th/Sc	2.34	0.04~0.05	0.83~20.00	1.00	0.03
Cr/Th	1.69	22.00~100.00	0.50~7.70	3.30	222.00
Co/Th	0.82	7.10~8.30	0.22~1.50	0.90	33.00
Data Source	In this paper	Cullers et al. [57]		Taylor and McLennan [6]	

4.2.3. Rare Earth Elements

The total content of the REEs (ΣREE) in the Yaojia Formation samples ranges from 91.65 to 207.98 ppm (avg. 134.23 ppm). Specifically, the LREE content ranges from 80.27 to 184.67 ppm (avg. 119.21 ppm), whereas the HREE content varies from 11.38 ppm to 23.31 ppm (avg. 15.02 ppm). The ratio of LREE/HREE varies between 6.91 and 8.93 (avg. 7.92) (Table 6), indicating that the LREEs are enriched, the HREEs are deficient, and the light and heavy REEs are highly fractionated.

The ratio of La_N/Yb_N varies between 6.62 and 9.58 (avg. 7.71), the ratio of La_N/Sm_N ranges from 3.17 to 4.37 (avg. 4.11), the ratio of Gd_N/Yb_N ranges from 1.06 to 1.58 (avg. 1.24), the δEu varies between 0.49 and 0.84 (avg. 0.57), whereas the δCe varies between 0.85 and 0.94 (avg. 0.89). Chondrite-normalized REE patterns are clearly right-sloping with obvious negative Eu anomalies (Figure 8a). The similarity between the curve patterns of each sample indicates that the REE content varies synchronously. In combination with the normalized REE distribution curve of the North American Shale (NASC), the characteristic curves of the samples are almost horizontal (Figure 8b). It is generally consistent with the characteristics of the NASC, which indicate that the source rocks of the Yaojia Formation originated from the UCC.

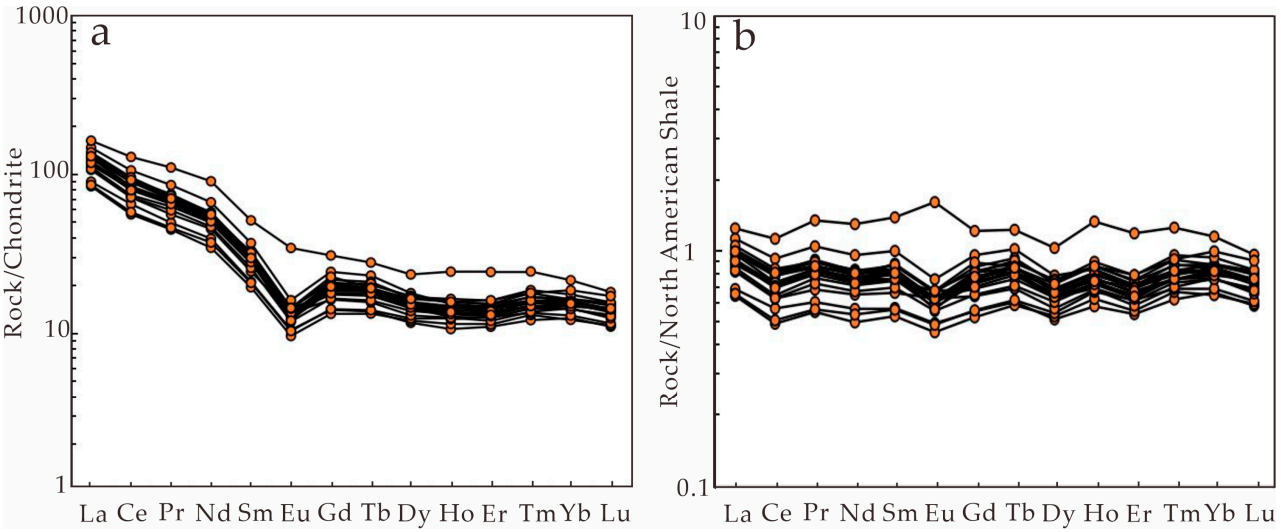


Figure 8. Chondrite-normalized REE patterns (**a**) and NASC-normalized REE patterns (**b**) of the Yaojia Formation in the SW Songliao Basin. The chondrite normalized data are quoted from Sun and McDonough [58]; the North American shale standardization data are quoted from Haskin and Paster [59].

Table 6. Data table of rare earth element analysis of the Yaojia Formation sandstones in the SW Songliao Basin (ppm).

Sample	La	Ce	Pr	Nd	Sm	Eu	Gd	Tb	Dy	Ho	Er	Tm	Yb	Lu	∑REE	LREE	HREE	L/H	La_N/Yb_N	La_N/Sm_N	Gd_N/Yb_N	δEu	δCe
KL051	29.30	52.10	6.52	24.30	4.29	0.71	3.75	0.69	3.77	0.81	2.40	0.44	2.61	0.36	132.05	117.22	14.83	7.90	7.58	4.30	1.16	0.53	0.87
KL052	30.80	53.40	6.58	25.20	4.48	0.74	3.84	0.69	3.99	0.84	2.43	0.41	2.67	0.39	136.46	121.20	15.26	7.94	7.79	4.33	1.16	0.53	0.86
KL053	31.70	58.40	7.03	27.30	4.76	0.77	4.18	0.72	3.89	0.80	2.24	0.38	2.55	0.36	145.08	129.96	15.12	8.60	8.39	4.19	1.32	0.52	0.90
KL054	31.10	57.00	6.68	26.40	4.70	0.78	4.04	0.69	3.64	0.72	2.07	0.37	2.33	0.33	140.85	126.66	14.19	8.93	9.01	4.17	1.40	0.53	0.91
KL056	21.90	41.30	4.76	18.60	3.24	0.61	2.86	0.51	2.95	0.60	1.82	0.31	2.05	0.28	101.79	90.41	11.38	7.94	7.21	4.26	1.13	0.60	0.93
KL057	20.50	35.60	4.32	16.30	2.99	0.56	2.70	0.50	3.04	0.65	1.88	0.33	2.00	0.28	91.65	80.27	11.38	7.05	6.92	4.32	1.09	0.59	0.87
KL058	20.90	36.80	4.43	17.60	3.19	0.60	2.89	0.52	3.14	0.69	2.09	0.34	2.13	0.29	95.61	83.52	12.09	6.91	6.62	4.12	1.10	0.59	0.88
KL059	27.00	47.00	6.02	23.40	4.23	0.79	3.57	0.64	3.64	0.76	2.20	0.37	2.49	0.35	122.46	108.44	14.02	7.73	7.32	4.02	1.16	0.62	0.85
KL060	35.90	67.30	8.22	31.50	5.67	0.93	4.96	0.86	4.53	0.86	2.42	0.40	2.53	0.34	166.42	149.52	16.90	8.85	9.58	3.99	1.58	0.52	0.91
KL061	39.70	81.80	10.60	42.70	7.88	1.99	6.29	1.04	5.94	1.38	4.02	0.63	3.55	0.46	207.98	184.67	23.31	7.92	7.55	3.17	1.43	0.84	0.94
KL062	32.30	59.30	7.20	27.00	4.91	0.82	4.42	0.79	4.20	0.89	2.51	0.43	2.71	0.39	147.87	131.53	16.34	8.05	8.04	4.14	1.32	0.53	0.90
KL063	31.00	56.70	6.82	25.80	5.00	0.83	4.24	0.75	4.35	0.89	2.54	0.46	2.69	0.38	142.45	126.15	16.30	7.74	7.78	3.90	1.27	0.54	0.90
KL066	28.60	50.80	6.44	24.30	4.55	0.77	4.18	0.77	4.28	0.93	2.66	0.48	2.89	0.40	132.05	115.46	16.59	6.96	6.68	3.96	1.17	0.53	0.87
KL067	28.90	53.10	6.40	25.40	4.61	0.74	4.00	0.72	4.01	0.78	2.37	0.39	2.62	0.36	134.40	119.15	15.25	7.81	7.45	3.95	1.23	0.52	0.90
KL068	27.90	51.40	6.39	24.90	4.28	0.77	3.91	0.72	3.95	0.83	2.34	0.40	2.57	0.35	130.71	115.64	15.07	7.67	7.33	4.10	1.23	0.57	0.89
KL069	26.00	45.50	5.38	21.40	3.76	0.77	3.32	0.59	3.28	0.71	1.98	0.35	2.36	0.32	115.72	102.81	12.91	7.96	7.44	4.35	1.14	0.65	0.88
KL070	26.30	45.70	5.71	22.10	3.96	0.69	3.37	0.60	3.50	0.75	2.12	0.38	2.34	0.32	117.84	104.46	13.38	7.81	7.59	4.18	1.16	0.56	0.86
KL071	28.80	50.50	6.25	23.90	4.31	0.83	3.64	0.67	3.68	0.79	2.28	0.38	2.43	0.36	128.82	114.59	14.23	8.05	8.00	4.21	1.21	0.62	0.87
KL072	33.50	60.90	7.05	26.50	4.94	0.84	4.62	0.72	3.84	0.77	2.16	0.41	2.53	0.36	149.14	133.73	15.41	8.67	8.94	4.27	1.48	0.53	0.91
KL073	31.70	58.60	6.77	26.40	4.57	0.70	4.01	0.72	4.17	0.89	2.67	0.46	3.07	0.43	145.16	128.74	16.42	7.84	6.97	4.37	1.06	0.49	0.92

4.3. Uranium Minerals

4.3.1. Uranium Mineral Types

A quantitative analysis of the electron microprobe (Table 7) indicates that the main uranium mineral type is pitchblende, with a small amount of coffinite. The content of UO_2 in pitchblende is very high, ranging from 71.34% to 81.60% (avg. 76.55%); SiO_2 content ranges from 0.99% to 4.81% (avg. 3.08%); TiO_2 content ranges from 0.62% to 3.90% (avg. 2.12%); and CaO content ranges from 0.89% to 3.84% (avg. 2.18%). In the study area, it is the mineral type with the highest content of uranium. The content of UO_2 in coffinite ranges from 59.36% to 69.31% (avg. 63.56%); the content of SiO_2 ranges from 11.66% to 18.93% (avg. 15.35%). There are small amounts of Al_2O_3, Y_2O_3, and FeO in coffinite. There is an average content of Al_2O_3, Y_2O_3, and FeO of 1.58%, 0.18%, and 2.10%, respectively. In comparison to pitchblende, coffinite has a relatively high SiO_2 content and a relatively low UO_2 content.

Table 7. Electronic probe analysis results of uranium minerals in the SW Songliao Basin (%).

Sites	MgO	Al_2O_3	SiO_2	TiO_2	UO_2	ZrO_2	CaO	Y_2O_3	PbO	MnO	FeO	Na_2O	BeO	P_2O_5	Total	Type
079-2	0	0.88	3.08	0.62	80.56	1.22	2.43	0.05	0	0.29	0.61	0.90	0.16	0.81	91.61	pitchblende
086-3	0.01	0.11	3.12	1.71	75.15	2.62	3.84	0.24	0	0.02	1.44	0.58	0	1.30	90.14	pitchblende
05A-1	0.05	0.66	0.99	0.95	81.60	1.14	0.96	0.06	0.03	0.12	3.07	0.83	2.60	0.48	93.54	pitchblende
05A-2	0.11	0.75	1.15	2.36	79.78	1.27	1.12	0.09	0	0.13	2.89	0.75	0.88	0.52	91.80	pitchblende
05A-6	0.06	0.45	4.81	2.74	75.88	1.08	0.89	0.01	0.05	0.07	2.80	0.50	0	0.58	89.92	pitchblende
74B-29	0	1.53	3.70	1.47	74.03	0.78	2.97	0.11	0.19	0.07	4.43	0.33	0	2.28	91.89	pitchblende
74A-14	0.24	3.26	3.43	3.90	71.34	1.02	3.72	0.09	0.02	0.14	0.82	0.68	0	1.42	90.08	pitchblende
24B-4	0.39	2.17	4.32	3.17	74.09	1.23	1.47	1.35	0.01	0	0.19	1.13	0.57	1.85	91.94	pitchblende
005-5	0.03	0.44	11.66	0.22	69.31	1.66	3.06	0.56	0.05	0	1.78	0.01	0	0.57	89.35	coffinite
024-4	0.22	1.27	15.06	1.06	65.02	0.41	0.63	0.03	0.04	0.07	2.52	0.32	1.19	0.18	88.02	coffinite
074-8	0.14	4.31	15.75	2.47	59.36	1.55	3.10	0.04	0	0.13	1.86	0.20	1.24	0.57	90.72	coffinite
074-20	0.06	0.31	18.93	1.40	60.56	0.75	2.55	0.08	0.07	0.10	2.25	0.64	0	1.53	89.23	coffinite

4.3.2. Characteristics of Uranium Minerals

Analysis of EMPA and BSE images in the study area reveals two primary forms of uranium present: independent uranium minerals and adsorption uranium. In general, their distribution patterns can be categorized as follows:

(1) Adsorption Uranium

Adsorption uranium is one of the most prevalent forms of uranium in the study area. Uranium is primarily absorbed by clay minerals in sandstone. A high content of clay minerals is preferable for uranium enrichment, as they have strong adsorption properties [60] (Figure 9a,b). Clay minerals are relatively abundant in the study area. In BSE images, uranium is adsorbed by clay minerals and distributed in vein or disseminated form.

(2) Uranium Minerals in Fissures and Dissolved Pores of Clastic Particles

The dissolution of detrital particles such as quartz and feldspar in an alkaline environment results in the formation of SiO_2, whereas the uranyl ion $(UO_2)^{2+}$ in oxygen-uranium bearing fluids reacts with the SiO_2 generated from detrital particles to produce coffinite [61]. Therefore, uranium minerals can be observed in BSE images distributed in the form of stellate, irregular granular, or vein, that fill in the fissures, edges, and dissolved pores of clastic particles (Figure 9c,d).

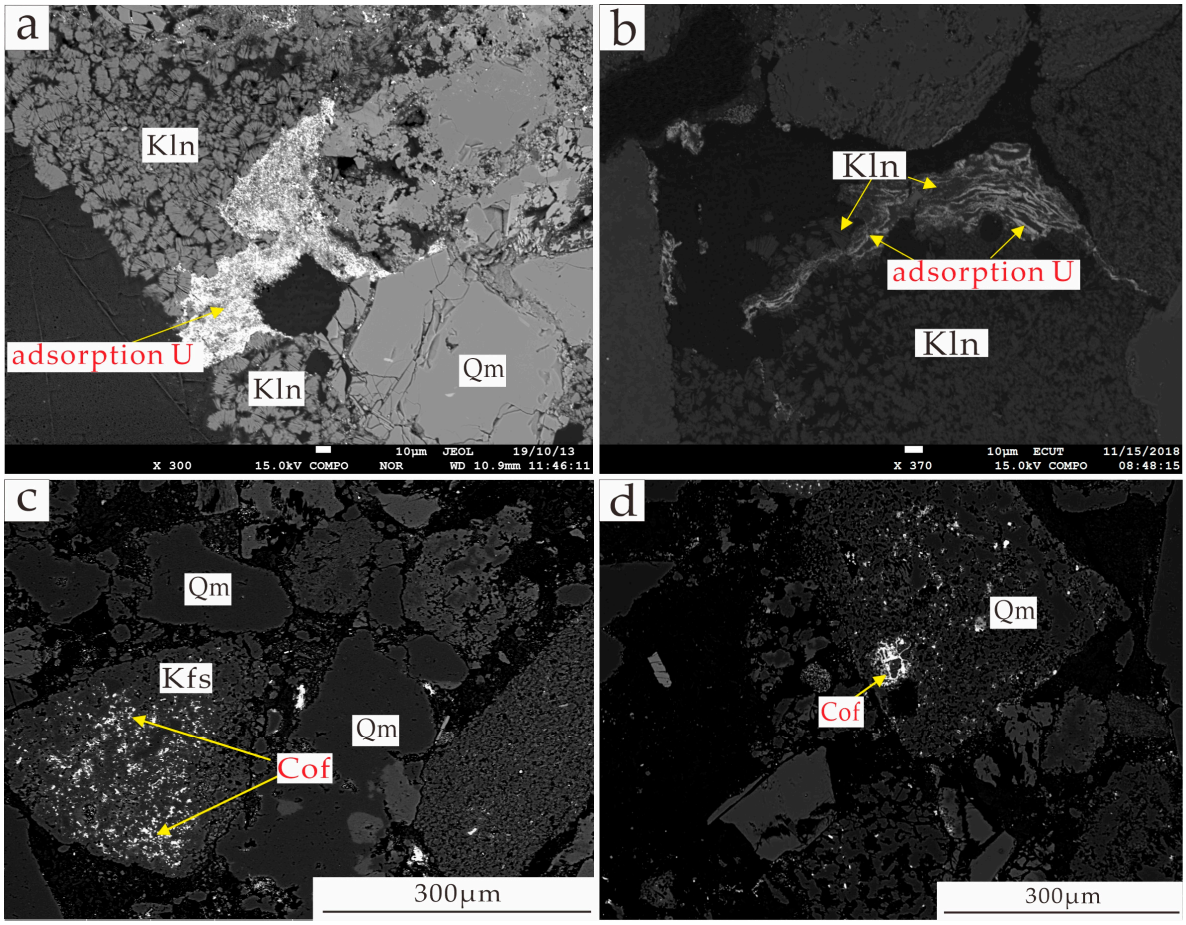


Figure 9. BSE images of uranium minerals in the Yaojia Formation sandstones. (**a**) Uranium is adsorbed by kaolinite; (**b**) uranium is adsorbed by kaolinite and distributed in the form of veins; (**c**) coffinite is distributed in stellate forms in the fissures and dissolved pores of k-feldspar; (**d**) coffinite fills in the dissolved pores of quartz. Abbreviations: Kln, kaolinite; Pit, pitchblende; Cof, coffinite; Kfs, k-feldspar; Qm, quartz.

(3) Uranium Minerals Associated with Pyrite

Observations from the field indicate that pyrite is highly developed around the ore stratum, which is closely linked to uranium mineralization. This is further demonstrated by BSE images, which show that a large number of uranium minerals are associated with pyrite, predominantly as pitchblende or coffinite developing around framboidal or colloidal pyrite (Figure 10a–c). It can be seen that pyrite and pitchblende are simultaneously generated in the organic matter cell cavity (Figure 10d). Under oxidizing conditions, uranium migrates in the hexavalent state (U^{6+}), whereas under reducing conditions, it precipitates toward the tetravalent state (U^{4+}) to form uranium minerals. Since pyrite is a potent reducing agent, it provides an excellent reducing environment for oxygenated uranium-bearing fluids. Pyrite and uranium minerals are in close symbiosis due to its ability to reduce U^{6+} in fluids to stable U^{4+}, enrich, and precipitate.

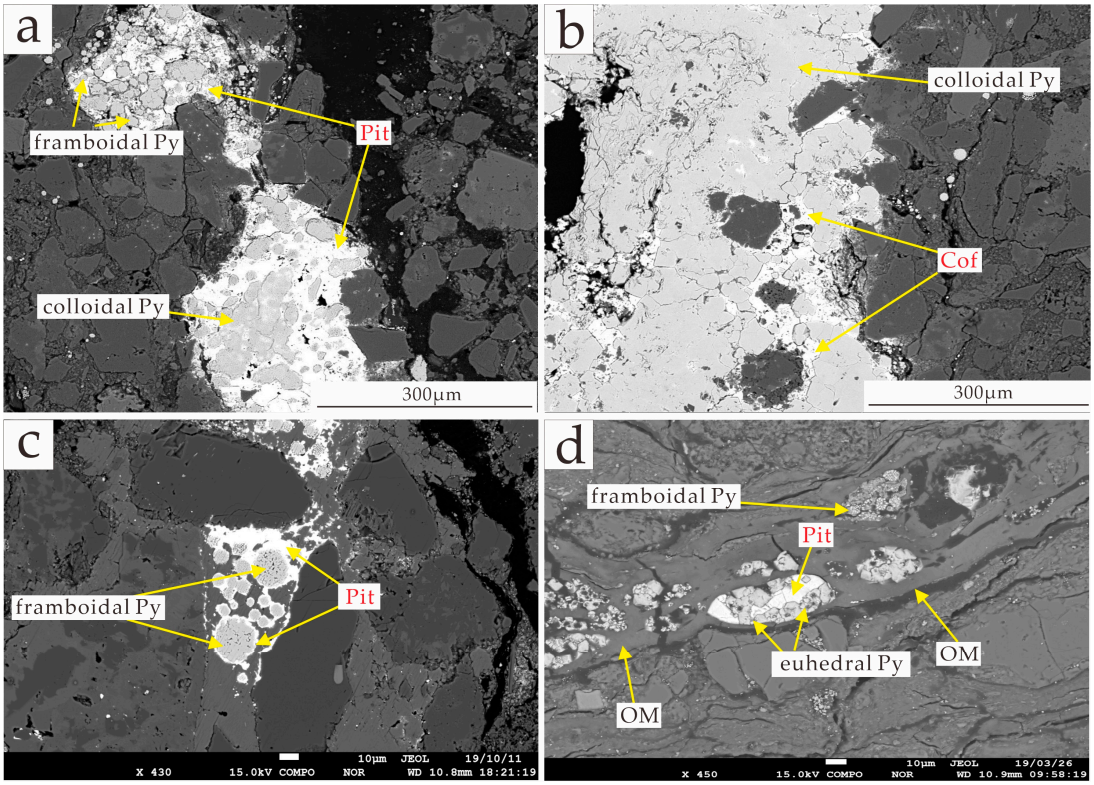


Figure 10. Characteristics of uranium minerals and pyrite in the Yaojia Formation sandstones. (**a**) Pitchblende grows around framboidal and colloidal pyrite. (**b**) Coffinite distributed in an irregular shape around colloidal pyrite. (**c**) Pitchblende distributed at the edges of the framboidal pyrite. (**d**) Pyrite and pitchblende are simultaneously generated in the organic matter cell cavity. Abbreviations: Pit, pitchblende; Py, pyrite; Cof, coffinite; OM, organic matter.

5. Discussion

5.1. Sedimentary Environment

During the depositional periods, certain multivalent trace elements are highly sensitive to changes in sedimentary environments, such as changes in the depth and salinity of paleosedimentary water and the redox conditions. They do not readily migrate during diagenesis, and the degree of enrichment of these elements in sediment is controlled by environmental conditions. Therefore, these elements and their ratios can be used as key indicators of sedimentary environments with a high degree of precision and accuracy [62–65]. The Sr/Ba, V/(V+Ni), V/Cr, Ni/Co, and (Cu+Mo)/Zn ratios are shown in Table 8.

The Sr/Ba ratio is typically used to evaluate the salinity of sedimentary water. In general, Sr content in freshwater environments ranges from 200 to 300 ppm, and in saltwater environments, it ranges from 800 to 1000 ppm [66]. As determined from the study of Sr/Ba ratios in terrestrial sedimentary basins in China, Sr/Br < 1 indicates a freshwater environment, whereas Sr/Ba > 1 indicates a saltwater environment [66]. The Sr content of all Yaojia Formation samples is below 300 ppm, except for six samples. The average Sr value is 223.94 ppm (n = 20). All samples, except one, have Sr/Ba ratios below 1, indicating that the Yaojia Formation was deposited in freshwater.

The elements V, Ni, Cr, and Co hardly migrate during diagenesis. They are readily soluble in oxidizing conditions but less soluble in reducing conditions. Thus, they preserve the original sedimentary records and serve as a marker for restoring the oxidation-reduction environment of paleo-water bodies [67]. In general, the V/(V+Ni) ratio is used to determine the intensity of bottom water body stratification during deposition [68]. A V/(V+Ni) ratio between 0.4 and 0.6 indicates weak stratification, between 0.6 and 0.84 implies moderate stratification, and a ratio above 0.84 denotes intense stratification. In the Yaojia Formation,

the V/(V+Ni) ratio varies between 0.62 and 0.95 (n = 20, avg. 0.82), which indicates a moderately stratified bottom water body with smooth circulation.

V and Cr share a similar characteristic in that they are readily enriched in sediments in reducing environments and readily soluble in water in oxidizing environments. Consequently, the V/Cr ratio is essential to determining redox conditions [69]. A V/Cr < 2.0 signifies an oxygen-rich environment, 2 < V/Cr < 4.25 denotes a sub-oxygen-rich environment, and V/Cr > 4.25 implies an anoxic environment [70]. With the exception of an abnormally high value (12.02), the V/Cr ratio of the Yaojia Formation sandstones ranges between 1.8 and 5.26 (n = 19, avg. 2.88), indicating that the Yaojia Formation was deposited in a sub-oxygenated environment.

According to Jones and Manning (1994) [70], a Ni/Co ratio below 5.00 indicates an oxygen-rich environment, between 5.00 and 7.00 indicates a sub-oxygen-rich environment, and higher than 7.00 implies an anoxic environment. Based on the Ni/Co ratios of the Yaojia Formation sandstone samples (0.99~2.46, avg. 1.65), it appears that they were deposited in an oxygen-rich environment.

Moreover, since the content of Cu and Zn in sediments is mainly controlled by redox and not influenced by diagenetic changes, the (Cu+Mo)/Zn ratio can also be used as an oxidation-reduction parameter. Lower values indicate a higher degree of oxidation [71]. Generally, a ratio of (Cu+Mo)/Zn less than 0.55 indicates a relatively oxygen-rich environment. The (Cu+Mo)/Zn ratio of the Yaojia Formation ranges from 0.05 to 1.21. The other values are all less than 0.55 except for the two high ones, which indicate a relatively oxygen-rich environment.

In conclusion, the Sr/Ba, V/(V+Ni), V/Cr, Ni/Co, and (Cu+Mo)/Zn ratios of these samples indicate that the Yaojia Formation was deposited in a sub- to oxygen-rich freshwater environment with a moderately stratified bottom water body.

Table 8. Trace element ratios of the Yaojia Formation sandstone samples in the SW Songliao Basin.

Sample	Sr/Ba	V/(V+Ni)	V/Cr	Ni/Co	(Cu+Mo)/Zn
KL051	0.29	0.82	2.37	1.83	0.13
KL052	0.29	0.81	2.54	1.71	0.12
KL053	0.33	0.81	2.02	1.70	0.15
KL054	0.32	0.80	1.80	1.65	0.22
KL056	1.15	0.74	4.69	1.56	0.06
KL057	0.80	0.64	3.18	1.42	0.05
KL058	0.63	0.62	3.07	1.43	0.05
KL059	0.30	0.84	3.41	1.46	0.12
KL060	0.48	0.90	2.19	2.46	0.15
KL061	0.10	0.74	5.26	1.15	0.82
KL062	0.31	0.87	2.40	1.66	0.15
KL063	0.27	0.86	2.84	1.11	0.16
KL066	0.38	0.95	12.02	1.36	0.10
KL067	0.30	0.89	4.41	0.99	0.25
KL068	0.27	0.81	3.01	2.00	1.21
KL069	0.47	0.83	2.20	1.62	0.18
KL070	0.38	0.83	2.20	1.83	0.15
KL071	0.27	0.80	2.34	1.92	0.10
KL072	0.28	0.85	2.24	1.96	0.23
KL073	0.19	0.92	2.55	2.14	0.48

5.2. Weathering-Alteration Degree

The discrimination of weathering-alteration degrees in sedimentary rocks is greatly affected by sedimentary recycling [72]. Therefore, it is necessary to evaluate the sedimentary recycling of samples before determining the degree of weathering-alteration. As weathered products from the source rocks are transported and deposited, sedimentary recycling may accumulate certain elements (Zr) and alter their composition [10]. Generally, both Th

and Sc are challenging to dissolve in water, and the Th/Sc ratio does not vary during sedimentary recycling. Therefore, it is frequently used to study compositional changes in source rocks [73]. Zircon is the most prevalent Zr-bearing mineral in sedimentary rocks. It is highly stable and accumulates in sediments as a result of sedimentary recycling. Zr/Sc will gradually increase with sedimentary recycling and zircon enrichment and will not be affected by late hydrothermal dilution [74]. Consequently, the Zr/Sc and Th/Sc ratios are used to determine the changes in sediment composition [75]. In the Zr/Sc-Th/Sc diagram (Figure 11a), the majority of sandstone sample spots are located along the compositional evolution line and exhibit strong positive correlations, indicating that the Yaojia Formation sediments have not undergone sedimentary recycling and are primarily controlled by source rocks. The $15Al_2O_3$-Zr-$300TiO_2$ diagram further supports this idea. In the $15Al_2O_3$-Zr-$300TiO_2$ diagram, the sandstone samples are situated close to the PAAS point with no changes in Al_2O_3/Zr ratios, suggesting the poor recycled nature of the Yaojia Formation sandstones and comparatively rapid deposition (Figure 11b) [76,77].

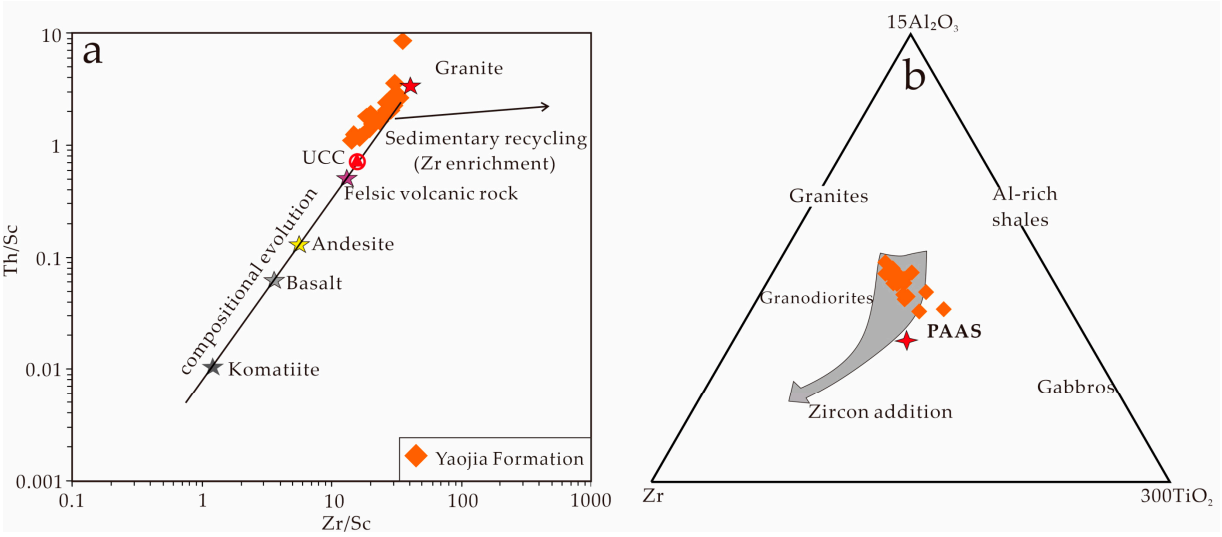


Figure 11. (**a**) Zr/Sc-Th/Sc diagram [75]; (**b**) $15Al_2O_3$-Zr-$300TiO_2$ diagram for the Yaojia Formation sandstones [76,77].

The content of unstable elemental oxides such as CaO, Na_2O, and K_2O in the sediments is closely linked to the chemical weathering of the source area and is commonly used to quantitatively evaluate the paleoweathering conditions of the source areas [73,78,79]. The Chemical Index of Alteration (CIA) can determine the degree of weathering-alteration in source rocks [54]. The CIA trend may also be indicative of paleoclimate characteristics during the deposition period. CIA values of 50–60 indicate low weathering intensity with a cold and dry climate; CIA values of 60–80 imply moderate weathering intensity with a warm and humid climate; and CIA values of 80–100 denote intense weathering intensity with a hot and wet climate [28]. The formula for calculating CIA is: $CIA = \{n(Al_2O_3)/[n(Al_2O_3) + n(CaO^*) + n(Na_2O) + n(K_2O)]\} \times 100$ [54]. CaO* denotes only the CaO content of silicate minerals, excluding the CaO content in carbonate and apatite [80]. In this instance, an adjustment must be made to the measured CaO content when carbonates and apatite are present [80]. CaO* is calculated and corrected in this study using the following formula: $n(CaO\ remaining) = n(CaO) - n(P_2O_5) \times 10/3$ [54]. In the case where n(CaO remaining) is less than $n(Na_2O)$, n(CaO remaining) should be adopted as CaO*. Otherwise, $n(Na_2O)$ should be adopted as CaO*. The calculated CIA value of the samples by the formula is listed in Table 3. The CIA values vary between 58.41 and 74.8 (avg. 67.80), indicating moderate weathering intensity.

The Index of Compositional Variability (ICV) is expressed as follows: $ICV = [n(Fe_2O_3) + n(K_2O) + n(Na_2O) + n(CaO^*) + n(MgO) + n(MnO) + n(TiO_2)]/n(Al_2O_3)$ [56]. If ICV < 1,

the clastic rocks are abundant in clay minerals, indicating that the sediments underwent sedimentary recycling or were first deposited under intense weathering; otherwise, if ICV > 1, the clastic rocks contain few clay minerals, reflecting that the sediments were first deposited during tectonic activity [56,81,82]. Among the Yaojia Formation sandstone samples, ICV values range from 0.63 to 3.15 (avg. 1.09), but sixteen samples have ICV values that are less than 1. In accordance with the Zr/Sc-Th/Sc and $15Al_2O_3$-Zr-$300TiO_2$ diagrams (Figure 11), the Yaojia Formation sandstones have not been subjected to sedimentary recycling. The ICV values therefore indicate that the sandstones were first deposited under intense weathering. The Chemical Index of Weathering (CIW) is used to measure the degree of chemical weathering in the provenance. The CIW is calculated as follows: $CIW = \{n(Al_2O_3)/[n(Al_2O_3) + n(CaO^*) + n(Na_2O)]\} \times 100$ [55]. A value greater than 85 indicates intense chemical weathering. The Yaojia Formation samples have CIW values varying between 74.52 and 95.74 (avg. 87.08). Both CIW and ICV demonstrate that the source rocks have been subjected to intense weathering.

As demonstrated by the CIA, ICV, and CIW indices, the source rocks of the Yaojia Formation have undergone moderate to intense weathering-alteration, and the palaeoclimate of the source area is generally humid and warm.

5.3. Source Rocks

The geochemical properties of sedimentary rocks are most indicative of their provenance characteristics [6]. Trace elements (such as Sc, Y, Zr, Nb, Hf, Th, etc.) in sedimentary rocks are commonly inactive, rarely changed, and difficult to dissolve in water during sedimentation [83–85]. Therefore, they may provide valuable information about the geochemical behavior of the source rocks and can be used to identify provenances. In addition, REEs are generally considered to be non-transportable. The REE content in sediments is generally restricted by the abundance of REE in the source rocks of the provenances. Transport, sedimentation, tectonic settings, and diagenesis have a limited impact on the REE content of sediments. The REE distribution patterns in sedimentary rocks will not be significantly altered by these processes. Therefore the presence of REE in sediments can provide a clear indication of the characteristics of the source rocks [6].

The TiO_2-Zr diagram can be used to differentiate between mafic, intermediate, and felsic igneous rocks as well as the components of the source rocks [86]. The Yaojia Formation sandstone samples have TiO_2 contents that vary between 0.18 and 0.58% (avg. 0.31%), while the Zr contents vary between 71.60 and 151.00 ppm (avg. 100.39 ppm). According to the TiO_2-Zr diagram, all Yaojia Formation sandstone samples are located in the felsic igneous rock region (Figure 12a). Generally, Sc, Ni, Cr, and Co tend to accumulate in basic rocks, while La, Th, Hf, Zr, and REE tend to accumulate in acidic rocks [57]. In the La/Sc-Co/Th diagram [84], the La/Sc ratios of the Yaojia Formation sandstones are widely dispersed (ranging from 4.14 to 12.29, avg. 7.34), whereas the Co/Th ratios are typically low, ranging from 0.16 to 2.54 (avg. 0.82). Most of the samples fall within the regions of felsic volcanic rock, granodiorite, and granite (Figure 12b) [84]. In the Th/Sc-Cr/Th diagram, the samples primarily fall within the region of felsic volcanic rock-granite (Figure 12c) [87]. In the La/Th-La/Yb diagram, the samples are located close to the region of the average upper crust (Figure 12d) [88]. The Yaojia Formation sandstones originated primarily from felsic igneous rocks of the UCC, based on the aforementioned characteristics. The REE content of the NASC is frequently used as an indicator of the REE compositional characteristics of the upper crust [6]. The NASC normalized REE distribution curves of the Yaojia Formation are nearly horizontal and close to unity (Figure 8b), indicating that the REE composition of the Yaojia Formation is comparable to that of the NASC and that the source rocks originated mainly from the UCC.

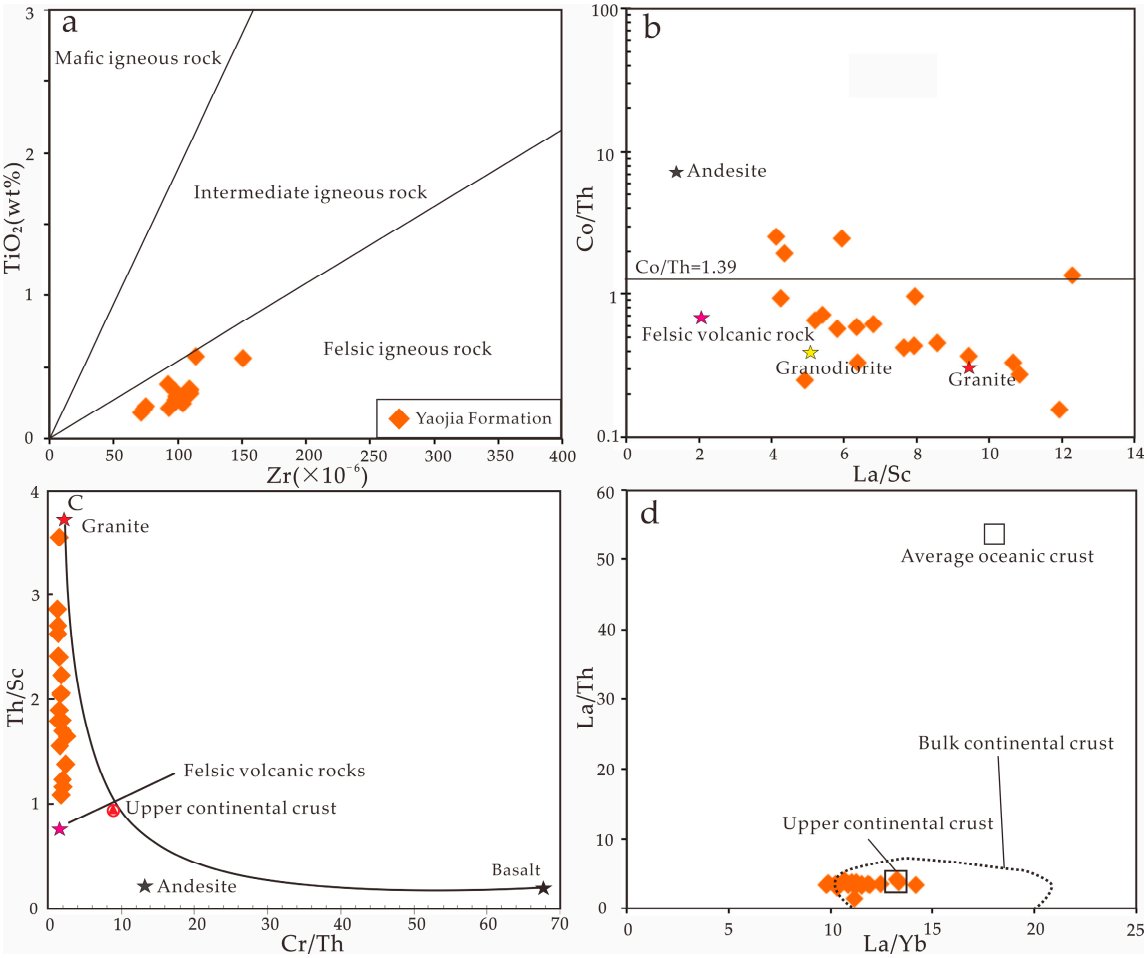


Figure 12. The source discrimination diagrams for the Yaojia Formation sandstones. (**a**) TiO_2-Zr diagram [86]; (**b**) La/Sc-Co/Th diagram [84]; (**C**) Th/Sc-Cr/Th diagram [87]; (**d**) La/Th-La/Yb diagram [88].

5.4. Tectonic Setting

The geochemical properties of sedimentary rocks may provide valuable insight into the composition of the source rock as well as the tectonic setting of the source areas [83,89]. Bhatia (1983, 1985) [89,90] classified basin tectonic types based on the character of the crust into four categories: oceanic island arc (OA), continental island arc (CA), active continental margin (ACM), and passive margin (PM). Major elements, such as Al_2O_3, SiO_2, TiO_2, $Fe_2O_3{}^T$, and MgO, have relatively high stability. In contrast, K_2O and Na_2O are highly unstable due to the considerable effects of potassium metasomatism and Na^+ loss during weathering, deposition, and diagenesis. Furthermore, calcite cement contributes the majority of the CaO content. Therefore, in this paper, the contents and ratios of the stable oxides Al_2O_3, SiO_2, TiO_2, $Fe_2O_3{}^T$, and MgO are used to distinguish source areas and tectonic settings. In the TiO_2-($Fe_2O_3{}^T$+MgO) diagram, the majority of the Yaojia Formation samples fall within the ACM field, with a tendency to the PM field, and three samples out of any of the fields (Figure 13a). The Al_2O_3/SiO_2-($Fe_2O_3{}^T$+MgO) diagram shows that samples mostly fall within the ACM region (Figure 13b).

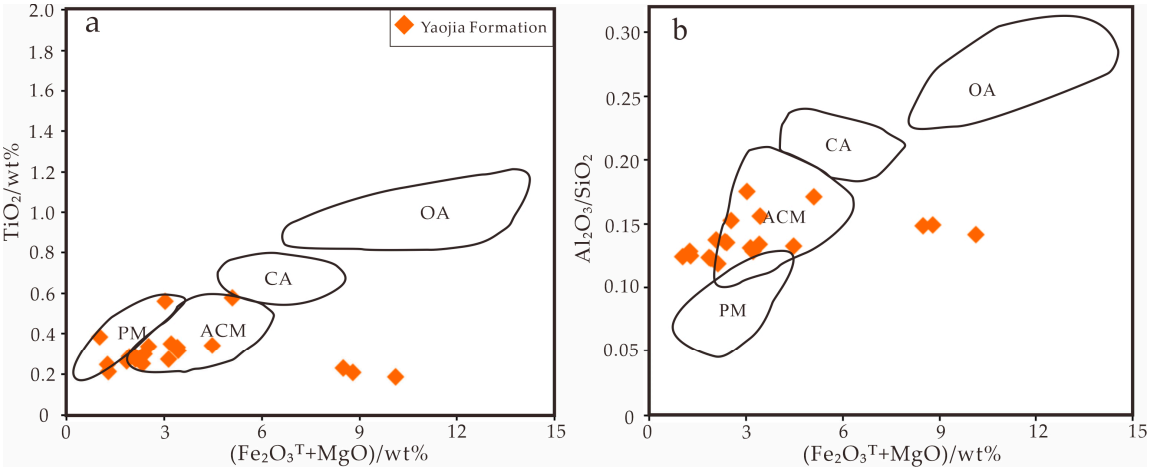


Figure 13. Major element discrimination diagrams of the Yaojia Formation sandstones for tectonic settings [89]. (**a**) TiO_2-($Fe_2O_3{}^T$+MgO) diagram; (**b**) Al_2O_3/SiO_2-($Fe_2O_3{}^T$+MgO) diagram.

A comparison of the geochemical characteristics of sandstones from the Yaojia Formation with those from various tectonic settings is presented in Table 9. Except for δEu, the ΣREE, LREE/HREE, La/Yb, and $(La/Yb)_N$ values in the Yaojia Formation are similar to their counterparts in the CA environment, while Nb, Y, Nd, V, Ni, Ba/Sr, and Nb/Y have similar characteristics to their counterparts in the ACM environment.

Table 9. Comparison of chemical compositions between the Yaojia Formation sandstones in the SW Songliao Basin and the sandstones from various tectonic settings (ppm).

	Research Region	OA	CA	ACM	PM
∑REE	134.23	58 ± 10	146 ± 20	186	210
LREE/HREE	7.92	3.8 ± 0.9	7.7 ± 1.7	9.10	8.50
La/Yb	11.42	4.2 ± 1.5	11 ± 3.6	12.5	15.9
$(La/Yb)_N$	7.71	2.8 ± 0.9	7.5 ± 2.5	9.10	8.50
δEu	0.57	1.04 ± 0.11	0.79 ± 0.13	0.60	0.56
Th	9.19	2.27 ± 0.7	1.11 ± 1.1	18.8 ± 3	16.7 ± 3
U	83.47	1.09 ± 0.21	2.53 ± 0.24	3.9 ± 0.5	3.2 ± 0.8
Zr	100.39	96 ± 20	229 ± 27	179 ± 33	298 ± 80
Nb	10.95	2.0 ± 0.4	8.5 ± 0.8	10.7 ± 1.4	7.9 ± 1.9
Y	23.36	19.5 ± 5.6	24.2 ± 2.2	24.9 ± 3.6	27.3 ± 5.3
Nd	25.05	11.36 ± 2.9	20.8 ± 1.6	25.4 ± 3.4	29.0 ± 5.03
V	50.18	131 ± 40	89 ± 13.7	48 ± 5.9	31 ± 9.9
Cr	14.58	37 ± 13	51 ± 6.5	26 ± 4.9	39 ± 8.5
Ni	10.56	11 ± 5.1	13 ± 2	10 ± 2.5	8 ± 4.4
Rb/Sr	0.59	0.05 ± 0.05	0.65 ± 0.33	0.89 ± 0.24	1.19 ± 0.4
Ba/Rb	6.83	21.3 ± 5.0	7.5 ± 1.3	4.5 ± 0.8	4.7 ± 1.1
Ba/Sr	3.30	0.95 ± 0.6	3.55 ± 1.4	3.8 ± 0.7	4.7 ± 1.3
Th/U	1.70	2.1 ± 0.78	4.6 ± 0.45	4.8 ± 0.38	5.6 ± 0.67
Zr/Th	11.84	48.0 ± 13.4	21.5 ± 2.4	9.5 ± 0.7	19.1 ± 5.8
Zr/Y	4.40	5.67 ± 1.94	9.6 ± 0.8	7.2 ± 0.4	12.4 ± 4.0
Nb/Y	0.47	0.11 ± 0.03	0.36 ± 0.04	0.43 ± 0.04	0.30 ± 0.06
Data Source	In this paper	Bhatia (1985) [90]; Bhatia and Crook (1986) [83]			

In general, trace elements (Co, Sc, Th, and Zr) and rare earth elements (La) are weakly active, and tectonic activity and diagenetic processes have a negligible effect on their fractionation during transport and deposition. Therefore, they may provide information about the original sediments as well as distinguish sedimentary tectonic settings [6,83,90,91]. In the La-Th-Sc diagram, the Yaojia Formation sandstone samples mainly fall within

the region of the ACM and PM (Figure 14a); in the Th-Sc-Zr/10 diagram and Th-Co-Zr/10 diagram, the samples mostly fall within the region of the ACM (Figure 14b,c).

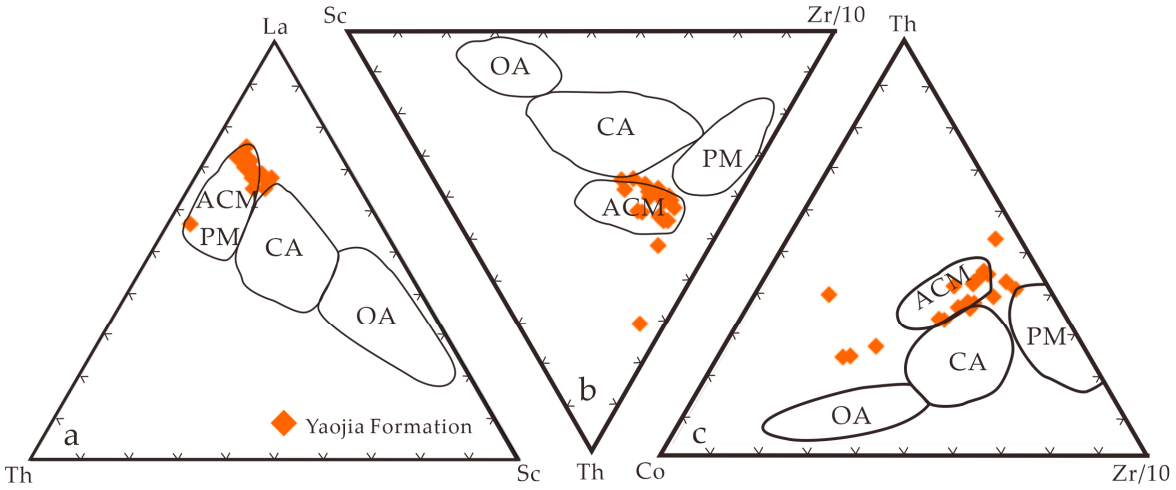


Figure 14. Trace element discrimination diagrams of the Yaojia Formation sandstones for tectonic settings [83]. (**a**) La-Th-Sc diagram; (**b**) Th-Sc-Zr/10 diagram; (**c**) Th-Co-Zr/10 diagram.

There is a direct correlation between the composition and geochemistry of the sedimentary rocks and the tectonic background of their provenances. The tectonic environment indicated by the geochemical characteristics of the samples in the above analysis reveals the tectonic background at the time of source rock formation [92], suggesting the complex tectonic background for the formation of rocks in the source area to some degree. Based on the results of the discrimination of the major and trace elements in the Yaojia Formation, the primary sources are upper crustal felsic igneous rocks in the ACM and CA environments.

5.5. Provenance Analysis

The Yaojia Formation in the SW Songliao Basin is characterized by sandy conglomerates, gray and gray-white medium- to coarse-grained sandstones, purplish-red siltstones, and reddish-purple mudstones [48]. Previous studies have identified the sedimentary environment as predominantly fluvial and deltaic facies [48], which are indicative of relatively strong hydrodynamic conditions. It is clear from the petrological and geochemical characteristics of the Yaojia Formation that it is a proximal deposition, with the source rocks being predominantly felsic igneous rocks. The sediments are mainly from recycled orogenic and transitional arc regions (Figure 6). Accordingly, the GXAM, ZGCM, and Kangfa Hilly areas adjacent to the SW Songliao Basin may be potential sources for the Yaojia Formation sediments.

The chemical characteristics of REEs in sedimentary rocks are similar. Since they can enter sediments rapidly and are difficult to migrate, they can preserve the geochemical characteristics of their source areas in the sediments [93]. As a result, REE characteristics are reliable indicators of sediment sources. The geochemistry of REEs in the Yaojia Formation sandstone exhibits enrichment of LREEs and depletion of HREEs. It is evident from Figure 8a that the partition curve exhibits a right-sloping type with obvious negative Eu anomalies. To further identify the main provenance of the Yaojia Formation sandstones during the deposition period, this paper conducted a statistical analysis of the REE partitioning pattern of igneous rocks from potential provenances around the SW Songliao Basin and compared the results with those of the sandstones from the study area [94–111]. As shown in Figure 15, the Yaojia Formation sandstones have similar REE partitioning patterns to those of the igneous rocks from the GXAM. Both exhibit a right-sloping type with obvious negative Eu anomalies, suggesting a close relationship between the sandstones of the study area and the igneous rocks of the GXAM. Accordingly, the sediments of the Yaojia Forma-

tion may have originated from felsic igneous rocks within the southern GXAM, which is consistent with their geographical location.

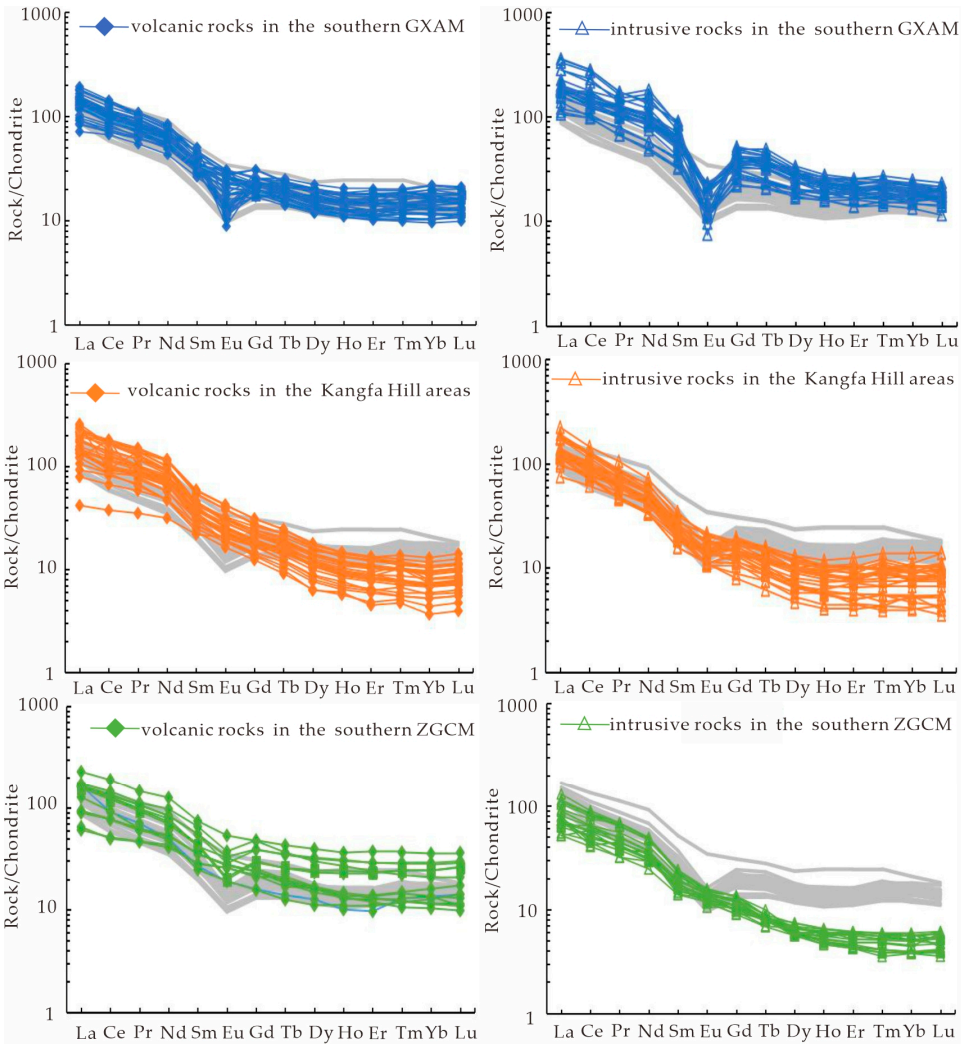


Figure 15. Chondrite-normalized REE patterns of igneous rocks distributed in potential provenances.

The GXAM are part of the Xing'an-Mongolian Orogenic Belt [99,112–114], which has undergone complex tectonic evolution during the Paleozoic and Mesozoic periods. During the Paleozoic, the GXAM experienced the tectonic evolution of the collocation of multiple microlandmasses in the Paleo-Asian tectonic domain. During the Mesozoic, the GXAM experienced the south-eastward subduction of the Mongolian Okhotsk ocean plate [115]. The GXAM is characterized by the large-scale distribution of Mesozoic and Paleozoic igneous rocks. The igneous rocks exposed in the GXAM consist primarily of granite, rhyolite, monzogranite, and granodiorite, with ages ranging from 120 to 165 Ma [37,99,104,113–121] and 240–280 Ma [108,122–128]. They have the properties of ACM and CA tectonic settings [28,113,129,130]. This is consistent with what the geochemical parameters of the Yaojia Formation sandstone samples show about the tectonic background. Zang et al. [131] determined that the detrital zircons of the Yaojia Formation sandstones are concentrated at 110 to 140 Ma and 240 to 260 Ma, respectively. This is generally consistent with the ages of igneous rocks exposed in the southern GXAM, thereby confirming the provenance of the Yaojia Formation. Based on the petrography, geochemistry, and previous detrital zircon U-Pb age evidence, it can be inferred that the Yaojia Formation sandstones in the SW Songliao Basin primarily originated from Late Paleozoic and Mesozoic felsic igneous rocks from the southern GXAM.

In general, uranium sources for sandstone-type uranium deposits are distributed in the provenance area, the sedimentary cover, and the ore-bearing strata themselves [26]. Thus, the felsic igneous rocks exposed in the southern GXAM may serve as a significant source of uranium mineralization. According to Zhang (2006) [25], the igneous rocks in the southern GXAM are highly abundant in uranium, with uranium content ranging from 5.2 to 9.1 ppm, which is substantially greater than the average uranium content of the upper crust (2.8 ppm) [6]. Furthermore, the uranium leaching rate of the igneous rocks in the southern GXAM ranged from 6.55% to 37.5%, with an average of 21.85%, reflecting the phenomenon of uranium migration [25]. Consequently, the igneous rocks of the source areas are uranium-rich and have a high rate of uranium leaching, making them a favorable external uranium source for the Yaojia Formation.

In the Late Cretaceous, the upper mantle of the Songliao region gradually chilled due to the westward subduction of the Pacific Plate and the weakening of thermal convection [41]. The lithospheric temperature of the Songliao Basin gradually decreased, resulting in thermal precipitation. As a result, the study area entered a period of large-scale depression. During this period, the GXAM experienced rapid uplift (97–90 Ma) [132]. Moreover, northeastern China experienced an O_2-rich environment at 91 Ma [132], which resulted in intense chemical weathering and denudation of igneous rocks in the southern GXAM, providing sufficient uranium-rich clastic materials for the Yaojia Formation. The clastic materials were transported by surface water to the basin for sedimentation, which resulted in uranium pre-enrichment in the Yaojia Formation. Subsequently, at the end of the formation of the Nenjiang Formation, the Songliao Basin was tectonically reversed by extrusion, and the Yaojia Formation was uplifted and exposed to the surface [30]. In the meantime, atmospheric precipitation leached uranium from the source rocks in the provenances. As a result, a large amount of oxygenated uranium-bearing fluids was produced and transported to the ore-bearing target layer along the basin boundary, providing the ore bodies with the necessary uranium for mineralization. The Yaojia Formation is characterized by an abundance of pyrite and organic matter, which provides a rich source of reductants for uranium mineralization [133]. This allows the U^{6+} in oxygenated uranium-bearing fluids to be continuously reduced to form pitchblende and coffinite [134], while remaining closely symbiotic with pyrite and organic matter. Additionally, the abundant clay minerals in the Yaojia Formation play a significant role in uranium mineralization since they can adsorb uranium in the fluids, resulting in the formation of adsorption uranium.

6. Conclusions

According to the petrography study, whole-rock geochemical analysis, and electron probe analysis of the Yaojia Formation sandstones in the SW Songliao Basin, the following conclusions can be drawn:

1. Pitchblende is the predominant uranium mineral in the study area, along with some coffinite. Uranium minerals are closely related to pyrite, organic matter, and clay minerals.
2. The Sr/Ba, V/(V+Ni), V/Cr, Ni/Co and (Cu+Mo)/Zn ratios of the samples indicate that the Yaojia Formation was deposited in a sub- to oxygen-rich freshwater environment with a moderately stratified bottom water body and smooth circulation.
3. In accordance with the Zr/Sc-Th/Sc and $15Al_2O_3$-Zr-$300TiO_2$ diagrams, the Yaojia Formation sediments have not undergone sedimentary recycling and are primarily controlled by source rocks. The CIA, ICV, and CIW values suggest that the source rocks have experienced moderate to intense weathering.
4. Based on the detrital components and geochemical characteristics of the Yaojia Formation samples, it is concluded that the Yaojia Formation sediments primarily originated from felsic igneous rocks in the upper crust under the tectonic settings of ACM and CA. The Mesozoic and Late Paleozoic felsic igneous rocks exposed in the southern GXAM are the main sources.

5. As well as providing sediments to the study area, the uranium-rich felsic igneous rocks in the southern GXAM also provided a long-term, stable, and ideal source of uranium. The uranium in the source rocks was transported to the sedimentary basin by oxygenated uranium-bearing fluids and precipitated into the ore-bearing layers.

Author Contributions: Conceptualization, F.N.; Funding acquisition, F.N. and D.Y.; Writing-original draft preparation, M.C.; Investigation and sampling, F.X., Z.Y. and D.Y. All authors have read and agreed to the published version of the manuscript.

Funding: This study was supported by the National Natural Science Foundation of China (Grant Nos. U2244205, U2067202, 41772068, and 42202095).

Data Availability Statement: Data is contained within the article.

Acknowledgments: We thank Geological Team No. 243 of the CNNC for the help in field sampling.

Conflicts of Interest: The authors declare no conflict of interest.

References

1. Naiman, Y. The detrital record of orogenesis: A review of approaches and techniques used in the Himalayan sedimentary basins. *Earth-Sci. Rev.* **2006**, *74*, 1–72.
2. Dickinson, W.R.; Gehrels, G.E. Sediment Delivery to the Cordilleran Foreland Basin: Insights from U-Pb Ages of Detrital Zircons in Upper Jurassic and Cretaceous Strata of the Colorado Plateau. *Am. J. Sci.* **2008**, *308*, 1041–1082.
3. Moreno, C.J.; Horton, B.K.; Caballero, V.; Mora, A.; Parra, M.; Sierra, J. Depositional and provenance record of the Paleogene transition from foreland to hinterland basin evolution during Andean orogenesis, northern Middle Magdalena Valley Basin, Colombia. *J. South Am. Earth Sci.* **2011**, *32*, 246–263. [CrossRef]
4. Thomas, W.A. Detrital-Zircon Geochronology and Sedimentary Provenance. *Lithosphere* **2011**, *3*, 304–308. [CrossRef]
5. Pereira, M.F.; Gama, C.; Chichorro, M.; Silva, J.B.; Gutierrez-Alonso, G.; Hofmann, M.; Linnemann, U.; Gartner, A. Evidence for Multi-Cycle Sedimentation and Provenance Constraints from Detrital Zircon U-Pb Ages: Triassic Strata of the Lusitanian Basin (Western Iberia). *Tectonophysics* **2016**, *681*, 318–331. [CrossRef]
6. Taylor, S.R.; McLennan, S.M. *The Continental Crust: Its Composition and Evolution: An Examination of the Geochemical Record Preserved in Sedimentary Rocks*; Blackwell Scientific Publication: Oxford, UK, 1985; pp. 1–312.
7. McLennan, S.M.; Taylor, S.R. Sedimentary rocks and crustal evolution: Tectonic setting and secular trends. *J. Geol.* **1991**, *99*, 1–21. [CrossRef]
8. Meng, E.; Xu, W.L.; Pei, F.P. Permian bimodal volcanism in the Zhangguangcai Range of eastern Heilongjiang Province, NE China: Zircon U-Pb-Hf isotopes and geochemical evidence. *J. Asian Earth Sci.* **2011**, *41*, 119–132. [CrossRef]
9. Nagarajan, R.; Roy, P.D.; Kessler, F.L.; Jong, J.; Dayong, V.; Jonathan, M. An integrated study of geochemistry and mineralogy of the Upper Tukau Formation, Borneo Island (East Malaysia): Sediment provenance, depositional setting and tectonic implications. *J. Asian Earth Sci.* **2017**, *143*, 77–94. [CrossRef]
10. McLennan, S.M.; Taylor, S.R.; McCulloch, M.T.; Maynard, J.B. Geochemical and Nd-Sr isotopic composition of deep-sea turbidites: Crustal evolution and plate tectonic associations. *Geochim. Cosmochim. Acta* **1990**, *54*, 2015–2050. [CrossRef]
11. Adeigbe, O.C.; Jimoh, Y.A. Geochemical fingerprints: Implication for provenance, tectonic and depositional settings of lower Benue trough sequence, Southeastern Nigeria. *J. Environ. Sci.* **2013**, *3*, 115–140.
12. Ikhane, P.R.; Akintola, A.I.; Bankole, S.I.; Oyinboade, Y.T. Provenance studies of sandstone facies exposed near Igbile southwestern Nigeria: Petrographic and geochemical approach. *J. Geogr. Geol.* **2014**, *6*, 47–68.
13. Ji, H.J.; Tao, H.F.; Qiu, J.L.; Wei, H.Y. Provenance of Middle Jurassic clastic rocks from the Bogda area of Eastern Tianshan and its implications. *Int. Geol. Rev.* **2019**, *62*, 1319–1342. [CrossRef]
14. Song, Y.; Ren, J.; Stepashko, A.A.; Li, J. Post-rift geodynamics of the Songliao Basin, NE China: Origin and signifificance of T11 (Coniacian) unconformity. *Tectonophysics* **2014**, *634*, 1–18. [CrossRef]
15. Chen, X.; Fang, X.; Guo, Q.; Xia, Y.; Pang, Y.; Sun, Y. Re-disscussion on uranium metallogenesis in Qianjiadian Sag, Songliao Basin. *Acta Geol. Sin.* **2008**, *82*, 553–561. (In Chinese)
16. Rong, H.; Jiao, Y.Q.; Wu, L.Q.; Ji, D.M.; Li, H.L.; Zhu, Q.; Cao, M.Q.; Wang, X.M.; Li, Q.C.; Xie, H.L. Epigenetic alteration and its constraints on uranium mineralization from Qianjiadian uranium deposit, Southern Songliao Basin. *Earth Sci.* **2016**, *41*, 153–166. (In Chinese)
17. Lin, J.R.; Tian, H.; Dong, W.M.; Xia, Y.L.; Zheng, J.W.; Qi, D.N.; Yao, S.C. Original geochemical types and epigenetic alteration of rocks in prospecting target stratum for uranium deposit in the southeast of Songliao Basin. *Uran. Geol.* **2009**, *25*, 202–207. (In Chinese)
18. Luo, Y.; He, Z.B.; Ma, H.F.; Sun, X. Metallogenic characteristics of Qianjiadian sandstone uranium deposit in the Songliao Basin. *Miner. Dep.* **2012**, *31*, 391–400. (In Chinese)

19. Bonnetti, C.; Cuney, M.; Michels, R.; Truche, L.; Malartre, F.; Liu, X.D.; Yang, J.X. The multiple roles of sulfate-reducing bacteria and Fe-Ti oxides in the genesis of the Bayinwula roll front-type uranium deposit, Erlian Basin, NE China. *Econ. Geol.* **2015**, *110*, 1059–1081. [CrossRef]
20. Bonnetti, C.; Liu, X.D.; Yan, Z.B.; Cuney, M.; Michels, R.; Malartre, F.; Mercadier, J.; Cai, J.F. Coupled uranium mineralisation and bacterial sulphate reduction for the genesis of the Baxingtu sandstone-hosted U deposit, SW Songliao Basin, NE China. *Ore Geol. Rev.* **2017**, *82*, 108–129. [CrossRef]
21. Jiao, Y.Q.; Wu, L.Q.; Rong, H. Model of inner and outer reductive media within uranium reservoir sandstone of sandstone-type uranium deposits and its ore-controlling mechanism: Case studies in Daying and Qianjiadian uranium deposits. *Earth Sci.* **2018**, *43*, 459–474. (In Chinese)
22. Rong, H.; Jiao, Y.Q.; Wu, L.Q.; Wan, D.; Cui, Z.J.; Guo, X.J.; Jia, J.M. Origin of the carbonaceous debris and its implication for mineralization within the Qianjiadian uranium deposit, southern Songliao Basin. *Ore Geol. Rev.* **2019**, *107*, 336–352. [CrossRef]
23. Rong, H.; Jiao, Y.Q.; Liu, X.F.; Wu, L.Q.; Jia, J.M.; Cao, M.Q. Effects of basic intrusions on REE mobility of sandstones and their geological significance: A case study from the Qianjiadian sandstone-hosted uranium deposit in the Songliao Basin. *Appl. Geochem.* **2020**, *120*, 104665. [CrossRef]
24. Rong, H.; Jiao, Y.Q.; Wu, L.Q.; Zhao, X.F.; Cao, M.Q.; Liu, W.H. Effects of igneous intrusions on diagenesis and reservoir quality of sandstone in the Songliao Basin, China. *Mar. Pet. Geol.* **2021**, *127*, 104980. [CrossRef]
25. Zhang, Z.Q. *Study on Metallogenic Conditions of Upper Cretaceous System for In-Situ Leachable Sandstone Type Uranium Deposit in South Songliao Basin*; Northeastern University: Shenyang, China, 2006; pp. 54–56. (In Chinese)
26. Jiao, Y.Q.; Wu, L.Q.; Peng, Y.B. Sedimentary-tectonic setting of the deposition-type uranium deposits forming in the Paleo-Asian tectonic domain, North China. *Earth Sci. Front.* **2015**, *22*, 189–205. (In Chinese)
27. Xia, F.Y.; Jiao, Y.Q.; Rong, H.; Wu, L.Q.; Zhu, Q.; Wan, L.L. Geochemical characteristics and geological implication of sandstone from the Yaojia Formation in Qianjiadian uranium deposit, Southern Songliao Basin. *Earth Sci.* **2019**, *44*, 4235–4251. (In Chinese)
28. Xu, Z.L.; Wei, J.L.; Zeng, H.; Li, R.L.; Li, J.G.; Zhu, Q.; Zhang, B.; Cao, M.Q. Late Cretaceous palynoligical assemblage and its palaeoclimate record from Yaojia Formation in Qianjiadian Depression, Kailu Basin. *Earth Sci.* **2017**, *42*, 1725–1735. (In Chinese)
29. Shan, Z.B. Provenance analysis of the lower part of Yaojia Formation in the Qianjiadian uranium deposit of the southwestern Songliao Basin. *Chin. J. Geol.* **2020**, *55*, 1248–1265. (In Chinese)
30. Wang, D.P.; Liu, Z.J.; Liu, L. *Evolution of the Songliao Basin and Sea Level Rise and Fall*; Geological Publishing House: Beijing, China, 1994.
31. Zou, C.N.; Xue, S.H.; Zhao, W.Z.; Li, M.; Wang, Y.C.; Liang, C.X.; Zhao, Z.K.; Zhao, Z.Y. Depositional sequences and forming conditions of the Cretaceous stratigraphic-lithologic reserviors in the Quantou-Nenjiang Formation, South Songliao Basin. *Pet. Explor. Dev.* **2004**, *02*, 14–17. (In Chinese)
32. Chen, F.H.; Zhang, M.Y.; Lin, C.S. Sedimentary environments and uranium enrichment in the Yaojia Formation, Qianjiadian depression, Kailu Basin. *Sediment. Geol. Tethyan Geol.* **2005**, *03*, 74–79. (In Chinese)
33. Wang, C.; Feng, Z.; Zhang, L.; Huang, Y.; Cao, K.; Wang, P.; Zhao, B. Cretaceous paleogeography and paleoclimate and the setting of SKI borehole sites in Songliao Basin, northeast China. *Palaeogeogr. Palaeoclim. Palaeoecol.* **2013**, *385*, 17–30. [CrossRef]
34. Yu, J.J.; Wang, F.; Xu, W.L.; Gao, F.H.; Pei, F.P. Early Jurassic mafic magmatism in the Lesser Xing'an–Zhangguangcai Range, NE China, and its tectonic implications: Constraints from zircon U–Pb chronology and geochemistry. *Lithos* **2012**, *142–143*, 256–266. [CrossRef]
35. Ge, M.H.; Zhang, J.J.; Li, L.; Liu, K.; Ling, Y.Y.; Wang, J.M.; Wang, M. Geochronology and geochemistry of the Heilongjiang Complex and the granitoids from the Lesser Xing'an-Zhangguangcai Range: Implications for the late Paleozoic-Mesozoic tectonics of eastern NE China. *Tectonophysics* **2017**, *717*, 565–584. [CrossRef]
36. Chen, X.; Hu, R.Z.; Liu, L.; Zhang, D.H. Petrogenesis of Jurassic granites linked to crustal growth above the subduction zone in the Lesser Xing'an Range (LXR), NE China. *J. Asian Earth Sci.* **2023**, *243*, 105524. [CrossRef]
37. Niu, S.D.; Li, S.R.; Huizenga, J.M.; Santosh, M.; Zhang, D.H.; Zeng, Y.J.; Li, Z.D.; Zhao, W.B. Zircon U-Pb geochronology and geochemistry of the intrusions associated with the Jiawula Ag-Pb-Zn deposit in the Great Xing'an Range, NE China and their implications for mineralization. *Ore Geol. Rev.* **2017**, *86*, 35–53. [CrossRef]
38. Ji, Z.; Ge, W.C.; Yang, H.; Wang, W.H.; Zhang, Y.L.; Wang, Z.H.; Bi, J.H. Late Jurassic rhyolites from the Wuchagou region in the central Great Xing'an Range, NE China: Petrogenesis and tectonic implications. *J. Asian Earth Sci.* **2018**, *158*, 381–397. [CrossRef]
39. He, X.L.; Yu, Q.Y.; Liu, S.Y.; Yang, M.J.; Zhang, D. Origin of the Erdaohe Ag–Pb–Zn deposit, central Great Xing'an Range, northeast China: Constraints from fluid inclusions, zircon U-Pb geochronology, and stable isotopes. *Ore Geol. Rev.* **2021**, *137*, 104309. [CrossRef]
40. Wu, Y.D.; Yang, J.H.; Sun, J.F.; Wang, H.; Zhou, B.Q.; Xu, L.; Wu, B. Revisiting the Late Jurassic adakitic rocks in the Yanshan fold and thrust belts, North China Craton. Partial melts from thickened continental crust? *Lithos* **2022**, *430–431*, 106885. [CrossRef]
41. Gao, R.Q.; Cai, X.Y. *Formation Conditions and Distribution Law of Oil and Gas Fields in the Songliao Basin*; Petroleum Industry Press: Beijing, China, 1997; pp. 12–24.
42. Jahn, B.M.; Wu, F.; Chen, B. *Granitoids of the Central Asian Orogenic Belt and Continental Growth in the Phanerozoic*; Special Papers; Geological Society America: Boulder, CO, USA, 2000; Volume 350, pp. 181–193.
43. Li, S.Q.; Chen, F.; Siebel, W.; Wu, J.D.; Zhu, X.Y. Late Mezosoic tectonic evolution of the Songliao basin, NE China: Evidence from detrital zircon ages and Sr-Nd isotopes. *Gondwana Res.* **2012**, *22*, 943–955. [CrossRef]

44. Zhou, J.B.; Wilde, S.A.; Zhang, X.Z.; Liu, F.L.; Liu, J.H. Detrital zircons from Phanerozoic rocks of the Songliao Block, NE China: Evidence and tectonic implication. *J. Asian Earth Sci.* **2012**, *47*, 21–34. [CrossRef]
45. Ren, J.; Tamaki, K.; Li, S.; Zhang, J. Late Mesozoic and Cenozoic rifting and its dynamic setting in Eastern China and adjacent areas. *Tectonophysics* **2002**, *344*, 175–205. [CrossRef]
46. Wang, P.; Liu, W.; Wang, S.; Song, W. $^{40}Ar/^{39}Ar$ and K/Ar dating on the volcanic rocks in the Songliao basin, NE China: Constraints on stratigraphy and basin dynamics. *Int. J. Earth Sci.* **2002**, *9*, 331–340. [CrossRef]
47. Dong, T.; He, S.; Wang, D.; Hou, Y. Hydrocarbon migration and accumulation in the Upper Cretaceous Qingshankou Formation, Changling Sag, Southern Songliao Basin: Insights from integrated analyses of fluid inclusion, oil source correlation and basin modelling. *J. Asian Earth Sci.* **2014**, *90*, 77–87. [CrossRef]
48. Cai, C.F.; Li, H.T.; Li, K.K.; Jiang, L. Anaerobic oxidation of petroleum coupled with reduction of uranium mineralization: Cases from Dongsheng and Qianjiadian uranium deposits. *Pet. Geol. Exp.* **2008**, *30*, 518–521. (In Chinese)
49. Scott, R.W. Late Cretaceous chronostratigraphy (Turonian-Maastrichtian): SK1 core Songliao Basin, China. *Geosci. Front.* **2012**, *3*, 357–367. [CrossRef]
50. Zhao, B.; Wang, C.; Wang, X.; Feng, Z.Q. Late Cretaceous (Campanian) provenance change in the Songliao Basin, NE China: Evidence from detrital zircon U-Pb ages from the Yaojia and Nenjiang Formations. *Palaeogeogr. Palaeoclimatol. Palaeocl.* **2013**, *385*, 83–94. [CrossRef]
51. Dickinson, W.R.; Suczek, C.A. Plate tectonics and sandstone compositions. *Am. Assoc. Pet. Geol. Bull.* **1979**, *63*, 2164–2182.
52. Chen, F.; Hegner, E.; Todt, W. Zircon ages and Nd isotopic and chemical compositions of orthogneisses from the Black Forest, Germany: Evidence for a Cambrian magmatic arc. *Int. J. Earth Sci.* **2000**, *88*, 791–802. [CrossRef]
53. Zhou, J.X. *Quantitative Analysis of Silicate Minerals by Electron Probe Method*; Standards Press of China: Beijing, China, 2002; pp. 1–8. (In Chinese)
54. Nesbitt, H.W.; Young, G.M. Early proterozoic climates and plate motions inferred from major element chemistry of lutites. *Nature* **1982**, *299*, 715–717. [CrossRef]
55. Harnois, L. The CIW index: A new chemical index of weathering. *Sediment. Geol.* **1988**, *55*, 319–322. [CrossRef]
56. Cox, R.; Lowe, D.R.; Cullers, R.L. The influence of sediment recycling and basement composition on evolution of mudrock chemistry in the south-western United States. *Geochim. Cosmochim. Acta* **1995**, *59*, 2919–2940. [CrossRef]
57. Cullers, R.L.; Podkovyron, V.N. Geochemistry of the Mesoproterozoic Lakhanda shales in southeastern Yakutia, Russia: Implication for mineralogical and provenance control, and recycling. *Precambrian Res.* **2000**, *104*, 77–93. [CrossRef]
58. Sun, S.S.; McDonough, W.F. Chemical and isotopic systematics of oceanic basalts: Implications for mantle composition and processes. In *Magmatism in the Ocean Basalts: Implications of Mantle Composition and Processes*; Special Publications; Saunders, A.D., Norry, M.J., Eds.; Geological Society: London, UK, 1989; Volume 42, pp. 313–345.
59. Haskin, L.A.; Paster, T.P. Geochemistry and mineralogy of the rare earths. In *Handbook on the Physics and Chemistry of Rare Earths*; Elsevier: Amsterdam, The Netherlands, 1979; Volume 3, pp. 1–80.
60. Yi, C.; Han, X.Z.; Li, X.D.; Zhang, K.; Chen, X.L. Study on sandstone petrologic feature of the Zhiluo Formation and its controls on uranium mineralization in Northeastern Ordos Basin. *Geol. J. China Univ.* **2014**, *20*, 185–197. (In Chinese)
61. Miao, A.S.; Lu, Q.; Liu, H.F.; Xiao, P. Occurrence and formation of coffinite in ancient interlayer oxidizing zone of sandstone type U-deposit in Ordos Basin. *Bull. Geol. Sci. Tech.* **2009**, *28*, 51–58. (In Chinese)
62. Wang, Y.Y.; Wu, P. Geochemical criteria of sediments in the coastal area of Jiangsu and Zhejiang Provinces. *J. Tongji Univ.* **1983**, *4*, 82–90. (In Chinese)
63. Liu, G.; Zhou, D.S. Application of microelements analysis in identifying sedimentary environment: Taking Qianjiang Formation in the Jianghan basin as an example. *Pet. Geol. Exp.* **2007**, *29*, 307–310. (In Chinese)
64. Tian, S.H.; Yang, Z.S.; Hou, Z.Q.; Liu, Y.C.; Gao, Y.G.; Wang, Z.L.; Song, Y.C.; Xue, W.E.; Lu, H.F.; Wang, F.C.; et al. Geological Characteristics and Prospecting Potential of No.1 Vein in Linglong Fault Belt, Shandong Province. *Miner. Depos.* **2009**, *28*, 747–758. (In Chinese)
65. Ma, H.H.; Liu, C.Y.; Zhang, L.; Zhang, D.D.; Wang, W.Q.; Zhao, Y.; Gao, M.; Quan, X.Y. Geochemical characteristics and depositional environment implications of sedimentary rocks in the Chang 7 member of Yanchang Formation in the Ordos Basin. *Geoscience* **2019**, *33*, 872–882. (In Chinese)
66. Rimmer, S.M.; Thompson, J.A.; Goodnight, S.A.; Robl, T.L. Multiple controls on the preservation of organic matter in Devonian-Mississippian marine black shales: Geochemical and petrographic evidence. *Palaeogeogr. Palaeoclimatol. Palaeoecol.* **2004**, *215*, 125–154. [CrossRef]
67. Pattan, J.N.; Pearce, N.J.G.; Mislankar, P.G. Constrains in using cerium-anomaly of bulk sediments as an indicator of paleo bottom water redox environment: A case study from the Central Indian Ocean Basin. *Chem. Geol.* **2005**, *221*, 260–278. [CrossRef]
68. Hatch, J.R.; Levecthal, J.S. Rekationship between inferred redox potential of the depositional environment and geochemistary of the upper pennsylvanian (Missourian) stark shale member of the dennis limestone. Wabanusee Country Kansas, U.S.A. *Chem. Geol.* **1992**, *99*, 65–82. [CrossRef]
69. Piper, D.Z. Seawater as the source of minor elements in black shales, phosphorites and other sedimentary rocks. *Chem. Geol.* **1994**, *117*, 95–114. [CrossRef]
70. Jones, B.; Manning, D.A.C. Comparison of geochemical indices used for the interpretation of palaeoredox conditions in ancient mudstones. *Chem. Geol.* **1994**, *111*, 111–129. [CrossRef]

71. Hallberg, R.O. A geochemical method for investigation of paleoredox conditions in sediments. *Ambio Spec. Rep.* **1976**, *4*, 139–147.
72. Gaillardet, J.; Dupre, B.; Allegre, C.J. Geochemistry of large river suspended sediments: Silicate weathering or recycling tracer? *Geochim. Cosmochim. Acta* **1999**, *63*, 4037–4051. [CrossRef]
73. Johnsson, M.J.; Basu, A.C. *Processes Controlling the Composition of Clastic Sediments*; Special Paper; Geological Society of America: Boulder, CO, USA, 1993; Volume 284, pp. 1–19.
74. Lambeck, A.; Huston, D.; Maidment, D.; Southgate, P. Sedimentary geochemistry, geochronology and sequence stratigraphy as tools to typecast stratigraphic units and constrain evolution in the gold mineralised Palaeoproterozoic Tanami Region, Northern Australia. *Precambrian Res.* **2008**, *166*, 185–203. [CrossRef]
75. Mclennan, S.M.; Hemming, S.; Mcdaniel, D.K.; Hanson, G.N. *Geochemical Approaches to Sedimentation, Provenance and Tectonics*; Special Paper; Geological Society of America: Boulder, CO, USA, 1993; Volume 284, pp. 21–40.
76. Garcia, D.; Fonteilles, M.; Moutte, J. Sedimentary fractionations between Al, Ti, and Zr and the genesis of strongly peraluminous granites. *J. Geol.* **1994**, *102*, 411–422. [CrossRef]
77. Caracciolo, L.; Le Pera, E.; Muto, F.; Perri, F. Sandstone petrology and mudstone geochemistry of the Peruc-Korycany Formation (Bohemian Cretaceous Basin, Czech Republic). *Int. Geol. Rev.* **2011**, *53*, 1003–1031. [CrossRef]
78. Fedo, C.M.; Wayne Nesbitt, H.; Young, G.M. Unraveling the effects of potassium implications metasomatism in sedimentary rocks and paleosols, with implications for paleoweathering conditions and provenance. *Geology* **1995**, *23*, 921–924. [CrossRef]
79. Nesbitt, H.W.; Young, G.M. Prediction of some weathering trends of plutonic and volcanic rocks based on thermodynamic and kinetic considerations. *Geochim. Cosmochim. Acta* **1984**, *48*, 1523–1534. [CrossRef]
80. McLennan, S.M. Weathering and global denudation. *J. Geol.* **1993**, *101*, 295–303. [CrossRef]
81. Barshad, I. The effect of a variation in precipitation on the nature of clay minerals formation in soils from acid and basic igneous rocks. In Proceedings of the International Clay Conference, Jerusalem, Israel, 20–24 June 1966; Israel Program for Scientific Translations: Jerusalem, Israel, 1966; pp. 167–173.
82. Van de Damp, P.C.; Leake, B.E. Petrography and geochemistry of feldspathic and mafic sediments of the northeastern Pacific margin. *Trans. R. Soc. Edinb. Earth Sci.* **1985**, *76*, 411–449. [CrossRef]
83. Bhatia, M.R.; Crook, K.A.W. Trace element characteristics of graywacks and tectonic discrimination of sedimentary basins. *Contrib. Miner. Pet.* **1986**, *92*, 182–193. [CrossRef]
84. Condie, K.C. Chemical composition and evolution of the upper continental crust: Contrasting results from surface samples and shales. *Chem. Geol.* **1993**, *104*, 1–37. [CrossRef]
85. McLennan, S.M.; Hemming, S.R.; Taylor, S.R.; Eriksson, K.A. Early Proterozoic crustal evolution: Geochemical and Nd-Pb isotopic evidence from metasedimentary rocks, southwestern North America. *Geochim. Cosmochim. Acta* **1995**, *59*, 1153–1177. [CrossRef]
86. Hayashi, K.I.; Fujisawa, H.; Holland, H.D.; Ohmoto, H. Geochemistry of ~1.9Ga sedimentary rocks from northeastern Labrador, Canada. *Geochim. Cosmochim. Acta* **1997**, *61*, 4115–4137. [CrossRef] [PubMed]
87. Condie, K.C.; Wronkiewicz, D.J. The Cr/Th ratio in Precambrian pelites from the Kaapvaal Craton as an index of craton evolution. *Earth Planet. Sci. Lett.* **1990**, *97*, 256–267. [CrossRef]
88. Shao, L.; Stattegger, K. Sandstone petrology and geochemistry of the Turpan Basin (NW China): Implications for the tectonic evolution of a continental basin. *J. Sediment. Res.* **2001**, *71*, 37–49. [CrossRef]
89. Bhatia, M.R. Plate Tectonics and geochemical composition of sandstones. *J. Geol.* **1983**, *91*, 611–627. [CrossRef]
90. Bhatia, M.R. Rare elements geochemical of Australia Paleozoic graywacks and mudrocks: Provenance and tectonic control. *Sediment. Geol.* **1985**, *45*, 97–113. [CrossRef]
91. MeLennan, S.M. Relationships between the trace element composition of sedimentary rocks and upper continental crust. *Geochem. Geophys. Geosystems* **2001**, *2*, 2000GC000109.
92. Li, S.Y.; Li, R.W.; Meng, Q.R.; Wang, D.X. Radiometric dating of sediments derived from metamorphic rocks of the Dabie Orogenic Belt in the Jurassic and Early Cretaceous. *Prog. Nat. Sci.* **2006**, *16*, 194–202.
93. Nesbitt, H.W.; MacRae, N.D.; Kronberg, B.I. Amazon deep-sea fan muds: Light REE enriched products of extreme chemical weathering. *Earth Planet. Sci. Lett.* **1990**, *110*, 118–123. [CrossRef]
94. Li, W.P.; Li, X.H.; Lu, F.X. Genesis and geological significance for the middle Jurassic high Sr and low Y type volcanic rocks in Fuxin area of west Liaoning, northeastern China. *Acta Petrol. Sin.* **2001**, *17*, 523–532. (In Chinese)
95. Li, W.P.; Li, X.H.; Lu, F.X.; Zhou, Y.Q.; Zhang, D.G. Geological characteristics and its setting for volcanic rocks of early Cretaceous Yixian Formation in western Liaoning province, eastern China. *Acta Petrol. Sin.* **2002**, *18*, 193–204. (In Chinese)
96. Yu, Q.; Ge, W.C.; Yang, H.; Xing, D.H.; Zhang, Y.L. Zircon U-b chronology and geochemical characteristics of volcanic rocks from Wudaoling Formation in Zhangguangcai Range. *Glob. Geol.* **2013**, *32*, 707–716. (In Chinese)
97. Duan, P.X.; Li, C.M.; Liu, C.; Deng, J.F.; Zhao, G.C. Geochronology and geochemistry of the granites from the Jinchanggouliang gold deposit area in the Inner Mongolia and its geological sigificance. *Acta Petrol. Sin.* **2014**, *30*, 3189–3202. (In Chinese)
98. Yang, Y.; Liu, S.R.; Xiao, M.S.; Yang, Y.Z. Geochemical characteristics of the Mesozoic-Cenozoic in Kulunqi area and its geological significance. *Mineral. Petrol.* **2014**, *34*, 54–60. (In Chinese)
99. Yang, W.B.; Niu, H.C.; Cheng, L.R.; Shan, Q.; Li, N.B. Geochronology, geochemistry and geodynamic implications of the Late Mesozoic volcanic rocks in the southern Great Xing'an Mountains, NE China. *J. Asian Earth Sci.* **2015**, *113*, 454–470. [CrossRef]
100. Li, P.C.; Li, S.C.; Liu, Z.H.; Li, G.; Bai, X.H.; Wan, L. Formation age and tectonic environment of volcanic rocks from Manketouebo Formation in Linxi area, Inner Mongolia. *Glob. Geol.* **2016**, *35*, 77–88. (In Chinese)

101. Li, P.C.; Liu, Z.H.; Li, S.C.; Xu, Z.Y.; Li, G.; Guan, Q.B. Geochronology, Geochemistry, Zircon Hf isotopic characteristics and tectonic setting of Hudugeshaorong pluton in Balinyouqi, Inner Mongolia. *Earth Sci.* **2016**, *41*, 1995–2007. (In Chinese)
102. Zou, T.; Wang, Y.W.; Wang, J.B.; Zhang, H.Q.; Zhao, L.T.; Shi, Y.; Liu, Y.Z. Zircon U-Pb chronology and geochemistry of late Carboniferous alkali rich intrusive rocks in the Xiayingfang Area, Eastern Hebei Province, and its geological significance. *Acta Geol. Sin.* **2017**, *91*, 2423–2442. (In Chinese)
103. Li, W.W.; Chen, J.S.; Gao, Z.H.; Liu, M.; Li, B.; Yang, F. Geochronology and geochemistry of the early carboniferous granodiorites in Haladaokou area of Chifeng city: Geological implication. *Geol. Res.* **2020**, *29*, 213–223. (In Chinese)
104. Zhang, C.; Quan, J.Y.; Zhang, Y.J.; Liu, Z.H.; Li, W.; Wang, Y.; Qian, C.; Zhang, L.; Ge, J.T. Late Mesozoic tectonic evolution of the southern Great Xing'an Range, NE China: Evidence from whole-rock geochemistry, and zircon U-Pb ages and Hf isotopes from volcanic rocks. *Lithos* **2020**, *362–363*, 105409. [CrossRef]
105. Ji, G.Y.; Jiang, S.H.; Li, G.F.; Yi, J.J.; Zhang, L.L.; Liu, Y.F. Metallogenetic control of magmatism on the Maodeng Su-Cu deposit in the southern Great Xing'an Range: Evidence from geochronology, geochemistry, and Sr-Nd-Pb isotopes. *Geotecton. Et Metallog.* **2021**, *45*, 681–704. (In Chinese)
106. Zhang, L.S.; Sun, F.Y.; Li, B.H.; Qian, Y.; Zhang, Y.J.; Wang, L.; Wang, L.L. Petrogenesis and tectonic setting of granitoids in the Fu'anpu molybdenum deposit Lesser Xing'an-Zhangguangcai range metallogenic belt: Constraints from element geochemistry, zircon U-Pb geochronology and Sr-Nd-Hf isotopes. *Acta Geol. Sin.* **2021**, *95*. (In Chinese) [CrossRef]
107. Zhang, L.S.; Sun, F.Y.; Qian, Y.; Zhang, Y.J.; Wang, L.; Wang, L.L. Petrogenesis of Middle Jurassic granitoids in Houdaomu, Central Jilin Province: Implications for the growth of Proterozoic continental crust in the eastern CAOB. *Acta Petrol. Sin.* **2021**, *37*, 2051–2072. (In Chinese)
108. Chen, G.Z.; Wu, G.; Li, Y.L.; Li, T.G.; Liu, R.L.; Li, R.H.; Yang, F. Zircon U-Pb age and geochemistry of the Qianjinchang intrusion in the Southern Great Xing'an Range and its Geological Implications. *Geotecton. Et Metallog.* **2022**, *46*, 356–379. (In Chinese)
109. Ji, G.Y.; Jiang, S.H.; Zhang, L.S.; Liu, Y.F.; Zhang, L.L. Chronology and geochemical characteristics of the highly fractionated alkali feldspar granite from the Maodeng deposit in the southern Great Xing'an Range. *Acta Petrol. Sin.* **2022**, *38*, 855–882. (In Chinese)
110. Zhang, G.B.; Chen, X.K.; Zhao, Y. Geochronology, Geochemistry and Geological Significance of the Middle Jurassic Porphyritic Monzogranite in the Southern Zhangguangcai Range, Heilongjiang Province. *J. Jilin Univ.* **2022**, *52*, 1907–1925. (In Chinese)
111. Li, H.N.; Han, J.; Zhao, Z.H.; Yin, Z.G. Magma-mixing origin for the Early Jurassic intrusive rocks in the eastern Songnen-Zhangguangcai Range Massif, NE China: Evidence from geochronology, geochemistry and Hf-O-Sr-Nd isotopes. *Gondwana Res.* **2023**, *121*, 72–91. [CrossRef]
112. Xiao, W.J.; Zhang, L.C.; Qin, K.Z. Paleozoic accretionary and collisional tectonics of the eastern Tienshan (China): Implications for the continental growth of Central Asia. *Am. J. Sci.* **2004**, *304*, 370–395. [CrossRef]
113. Ouyang, H.G.; Mao, J.W.; Zhou, Z.H.; Su, H.M. Late Mesozoic metallogeny and intracontinental magmatism, southern Great Xing'an Range, northeastern China. *Gondwana Res.* **2015**, *27*, 1153–1172. [CrossRef]
114. Wang, P.; Chen, Y.J.; Wang, C.M.; Zhu, X.F.; Wang, S.X. Genesis and tectonic setting of the giant Diyanqin'amu porphyry Mo deposit in Great Hingan Range, NE China: Constraints from U-Pb and Re–Os geochronology and Hf isotopic geochemistry. *Ore Geol. Rev.* **2016**, *8*, 760–779. [CrossRef]
115. Xu, W.L.; Wang, F.; Fei, F.P.; Meng, E.; Tang, J.; Xu, M.J.; Wang, W. Mesozoic tectonic regimes and regional ore-forming background in NE China: Constrains from spatial and temporal variation of Mesozoic volcanic rock associations. *Acta Petrol. Sin.* **2013**, *29*, 339–353. (In Chinese)
116. Deng, C.Z.; Sun, D.Y.; Li, G.H.; Lu, S.; Tang, Z.Y.; Gou, J.; Yang, Y.J. Early Cretaceous volcanic rocks in the Great Xing'an Range: Late effect of a flat-slab subduction. *J. Geodyn.* **2019**, *124*, 38–51. [CrossRef]
117. Wang, D.; Zhao, G.C.; Su, S.G.; Li, H.X. Spatial-temporal distribution of Late Mesozoic intrusive rocks in south Daxing'anling Mountains and the characteristic contrast of rocks in the mid ridge and the east slope. *Geoscience* **2020**, *34*, 466–482. (In Chinese)
118. Chen, G.Z.; Wu, G.; Li, T.G.; Liu, R.L.; Li, R.H.; Li, Y.L.; Yang, F. Mineralization of the Daolundaba Cu-Sn-W-Ag deposit in the southern Great Xing'an Range, China: Constraints from geochronology, geochemistry, and Hf isotope. *Ore Geol. Rev.* **2021**, *133*, 104117. [CrossRef]
119. Liu, F.; Wang, X.; Hai, L.F.; Zhao, D.S. Zircon U-Pb ages, Hf isotope and extensional tectonics of manzogranite in the Hansumu area of southern Great Khingan. *Geol. China* **2021**, *48*, 1609–1622. (In Chinese)
120. Guo, X.G.; Li, J.W.; Li, C.J.; Jiao, T.L. Geochronology, geochemistry, and Sr–Nd–Pb–Hf isotopes of ore-related diorites in the Erdaohe Pb-Zn-Ag deposit, Great Hinggan Range, NE China: Constraints on timing, petrogenesis and tectonic setting. *Lithos* **2021**, *386–387*, 106005. [CrossRef]
121. He, P.; Guo, S.; Zhang, T.F.; Zhang, Y.L.; Su, H.; Fu, Q.L. Geochronology, geochemistry and tectonic setting of volcanic rocks from Manketouebo Formation in Wulagai area, southern Great Xing'an Range. *Geol. China* **2022**, *49*, 601–619. (In Chinese)
122. Guo, Z.J.; Zhou, Z.H.; Li, G.T.; Li, J.W.; Wu, X.L.; Ouyang, H.G.; Wang, A.S.; Xiang, A.P.; Dong, X.Z. SHRIMP U-Pb zircon dating and petrogeo-chemistral characteristics of the intermediate-acid intrusive rocks in the Aoergai copper deposit of Inner Mongolia. *Geol. China* **2012**, *39*, 1486–1500. (In Chinese)
123. Liu, J.; Xi, A.H.; Ge, Y.H.; Tang, X.Y.; Xu, B.W.; Wang, M.Z.; Ma, Y.J. LA-ICP-MS zircon U-Pb ages and petrogenesis of granodiorite in Mengguyingzi, Chifeng, Inner Mongolia. *Geol. China* **2015**, *34*, 437–446. (In Chinese)

124. Zhang, H.H.; Zheng, Y.J.; Chen, S.W.; Zhang, J.; Gong, F.H.; Su, F.; Huang, X. Age of Xingfuzhilu Formation and Contact Relation between Permian and Triassic strata in southern Da Hinggan Mountains: Constraints from the tuff zircon U-Pb ages. *Geol. Bull. China* **2015**, *42*, 1754–1764. (In Chinese)
125. Du, J.Y.; Tao, N.; Guo, J.C.; Jiang, B.; Du, G.X. Geochronology and Geochemistry of Bayanchagan Pluton in Balinyouqi, Inner Mongolia: Implication for Timing of closure of Paleo-Asian Ocean. *Earth Sci.* **2019**, *44*, 3361–3377. (In Chinese)
126. Li, M.X. Geochemical characteristics and petrogenesis of Early Cretaceous monzonitic granite in theMandu area, southern Da Hinggan Mountains. *Geol. Bull. China* **2020**, *39*, 224–233. (In Chinese)
127. Zhao, Q. *Magmatism and Leas-Zinc Mineralization in the Southern Great Xing'an Range, NE China*; China University of Geoscience: Beijing, China, 2020; pp. 56–77.
128. Zhang, L.L.; Jiang, S.H.; Bagas, L.; Kang, H. An ancient continental crustal source for Mo mineralisation in the eastern Central Asian Orogen: A case study of the Bilugangan Mo deposit. *Ore Geol. Rev.* **2021**, *139*, 104513. [CrossRef]
129. Zhang, D.Q. Two granitoid series in different tectonic environment of Souther Da Hinggan Mountains, China. *Acta Petrol. Mineral.* **1993**, *12*, 1–11. (In Chinese)
130. Liu, Y.J.; Zhang, X.Z.; Jin, W.; Chi, X.G.; Wang, C.W.; Ma, Z.H.; Han, G.Q.; Wen, Q.B.; Zhao, Y.L.; Wang, W.D.; et al. Late Paleozoic tectonic evolution in Northeast China. *Geol. China* **2010**, *37*, 943–951. (In Chinese)
131. Zang, Y.H.; Li, J.M.; Ning, J. Provenance tracing and tectonic setting of the Upper Cretaceous Yaojia Formation sandstone in the HLJ area, southern Songliao Basin: Constrains from petrogeochemistry and zircon U-Pb chronology. *Bull. Geol. Sci. Tect.* **2022**. (In Chinese)
132. Wang, S.Y.; Cheng, Y.H.; Xu, D.H. Late Cretaceous-Cenozoic tectonic-sedimentary evolution and U-enrichment in the southern Songliao Basin. *Ore Geol. Rev.* **2020**, *126*, 103786. [CrossRef]
133. Chen, M.Y.; Nie, F.J.; Fayek, M. Discussion of the genetic relationship between pyrite and uranium mineralization in sandstone-type uranium deposit in Kailu Basin. *Acta Geosci. Sin.* **2021**, *42*, 868–880. (In Chinese)
134. Huang, G.; Wu, D.; Huang, G.; Xue, W.; Min, Z.; Fan, P. Provenance of Jurassic Sediments from Yuqia Sandstone-Type Uranium Deposits in the Northern Margin of Qaidam Basin, China and Its Implications for Uranium Mineralization. *Minerals* **2022**, *12*, 82. [CrossRef]

Disclaimer/Publisher's Note: The statements, opinions and data contained in all publications are solely those of the individual author(s) and contributor(s) and not of MDPI and/or the editor(s). MDPI and/or the editor(s) disclaim responsibility for any injury to people or property resulting from any ideas, methods, instructions or products referred to in the content.